UPPSALA
UNIVERSITET

UPTEC K 21006
Examensarbete 30 hp
Mars 2021

Short wavelength UV–LED photoinitiated radical polymerization of acrylate–based coating systems—A comparison with conventional UV curing.

Olof Torfgård

UPPSALA
UNIVERSITET

Teknisk- naturvetenskaplig fakultet
UTH-enheten

Besöksadress:
Ångströmlaboratoriet
Lägerhyddsvägen 1
Hus 4, Plan 0

Postadress:
Box 536
751 21 Uppsala

Telefon:
018 – 471 30 03

Telefax:
018 – 471 30 00

Hemsida:
http://www.teknat.uu.se/student

Abstract

Short wavelength UV–LED photoinitiated radical polymerization of acrylate–based coating systems—A comparison with conventional UV curing.

Olof Torfgård

The present work was performed at Sherwin–Williams Sweden group AB with the objective of comparing short-wavelength light emitting diodes (UVB/UVC) with the conventional mercury arc lamp as a curing method of acrylate-based, UV-paint undergoing free-radical polymerization when exposed to UV-radiation. Due to environmental and health risks, mercury-doped radiation sources will be phased out in the near future, according to the United Nations Minamata convention, hence new alternatives are needed.
Light-emitting diodes differ from the mercury arc lamp as they provide semi-discrete output intensity lines within the UV spectrum instead of a broad output distribution with several main intensity lines. The power output is also considerably lower compared to the conventional method which limits the irradiance and dose that are key parameters in activating and propagating free-radical polymerization of UV-paint.
Seven different light-emitting diodes between 260–320 nm was examined and compared to the conventional mercury arc lamp.
Cured coatings were evaluated by measuring the relative extent of acrylate conversion with ATR-FTIR and micro-hardness indentation test. Both methods correlate to the relative cross-linking density and qualitatively describe the curing process for each radiant source at a specific irradiance and dose.
Three different paint formulations with widely different properties were used in the experiments. All three paints were able to cure with one or several light emitting diodes at comparable doses and 10 to 20 times lower irradiance to the conventional mercury arc lamp, resulting in similar acrylate conversion and hardness.

Handledare: Rickard Drougge
Ämnesgranskare: Jonas Mindemark
Examinator: Peter Broqvist
ISSN: 1650-8297, UPTEC K 21006
Tryckt av: Uppsala

Populärvetenskaplig sammanfattning

Sherwin–Williams är en producent av polymera ytbehandlingssystem, bland annat industriell färg som tillverkas i fabriken i Arlanda stad. Ultraviolett-härdande färg är en typ av produkt som riktar sig framförallt mot beläggning av möbler och golv. Färgen torkar på tusendelar av en sekund då den exponeras av UV-ljus vid specifika energier och våglängder. Denna typ av härdningsteknik är mycket lämplig i industriellt syfte då stora volymer av möbler eller golv kan tillverkas snabbt och direkt staplas för lagring, vidare bearbetas eller förpackas tack vare den snabba torktiden. Den konventionella ljuskällan för UV-ljuset är ett typ av ljusrör innehållandes kvicksilver. Kvicksilvret är nödvändigt för att erhålla rätt egenskaper på det utgående ljuset som härdar färgen.

Enligt Förenta nationernas Minamata-konvention ska kvicksilver fasas ut då det är skadligt för både hälsan och miljön. Därav letar man efter alternativa ljuskällor där ljusdioder (LED) är en möjlig kandidat. Distributionen av UV-ljus från en LED emitteras i semi-diskreta intensitetslinjer i UV-spektrumet (200–400 nm) medan ett kvicksilverrör ger ut ljus i flera intensitetslinjer samtidigt i UV-spektrumet. Dessutom är det en mycket lägre energi på det utgående ljuset från en LED jämfört med från ett kvicksilverrör. En viss irradians behövs för att torkprocessen av färgen ska initieras och en viss dos för genomhärdning så att beläggningen erhåller rätt materiella egenskaperna som till exempel kemikalieresistans, hårdhet, vidhäftning etc.

Irradians mäts i bestrålning per ytarea, i detta fall effekten (W) av UV-ljuset per ytenhet beskrivet i [mW/cm^2] och dos beskrivs som [mJ/cm^2] där en Joule (J) motsvarar arbetet som krävs för att producera en watt under en sekund, det vill säga en wattsekund ($J=W\times s$) och har således ett tidsberoende.

För att undersöka om LED har potentialen att helt ersätta kvicksilverröret som ljuskälla i framtiden, har tre kommersiella produkter från Sherwin–Williams undersökts i den här studien. En transparent topplack, en pigmenterad toppfärg och en pigmenterad grundfärg som tillsammans representerar en bred täckning av de olika produktfamiljerna och deras egenskaper.

Mätningar av de härdade filmernas hårdhet utfördes med en mikro-hårdhetsmätare och den relativa tvärbindningsdensiteten mättes med ATR-FTIR. Båda metoderna ska i teorin indikera hur väl beläggningen av färgen har härdats efter belysning. Korrelationen mellan båda metoderna visade sig vara hög och påvisade väl graden av härdning i de olika beläggningarna.

Resultaten visade på att ljusdioderna hade ungefär 15–20 gånger lägre irradians från ett avstånd av 5,3 mm jämfört med kvicksilverröret från 150 mm. Dock var denna relativt låga irradiansen tillräcklig för att initiera härdning. Dosen gick att jämföra i samma storleksordning då substraten med färg var i fixerat läge då ljusdioderna användes. Detta på grund av tidsberoendet för dosen. Vid jämförbara doser och högsta möjliga irradians var härdningen med ljusdioder jämförbar med kvicksilverröret som konventionell metod för en eller flera våglängder vilket är mycket lovande för ljusdioder som härdningsmetod i framtiden. Det kunde dock konstateras att ljusdioderna inte är tillräckligt starka idag för att fungera praktiskt i ett industriellt sammanhang då avståndet mellan ljuskälla och substrat sannolikt behöver vara större än 5,3 mm. Dessutom färdas substraten på transportband med hastigheter som ofta kan var upp emot 40 m/min eller ännu högre hastigheter. Detta har således en stor inverkan på det tidsförlopp som färgen belyses och dosen minskar med bandhastigheten.

Abbreviations and Definitions

Abbreviations

UV – Ultraviolett

LED – Light-Emitting Diode

ATR-FTIR – Attenuated Total Reflectance – Fourier Transform Infrared

M_w – Average molecular weight

D_t – Tracer diffusion coefficient

R_h – Hydrodynamic radius

η_s – Solvent viscosity

T_g – Glass transition temperature

T_{cure} – Ambient curing temperature

E_n – Irradiance

I – Radiant intensity

P_{out} – Power output (radiant flux)

HM – Martens hardness

Definitions

η_i – *Internal quantum efficiency*: "Proportion of all electron–hole recombination's in the active region that are radiative, producing photons".

η_e – *Extraction quantum efficiency*: "Proportion of photons generated in the active region that escape from the device".

η_{ext} – *External quantum efficiency*: "The ratio of the number of photons emitted from the LED to the number of electrons passing through the device, i.e., how efficiently the device converts electrons to photons and allows them to escape".

Contents

Populärvetenskaplig sammanfattning i
Abbreviations and Definitions ii
1. Introduction 1
2. Objective 1
3. Theory 2
3.1 Complexity of UV paint formulations 2
3.2 Principles of ultraviolet initiation of curing 3
3.2.1 Free-radical chain polymerization 3
3.2.2 Photoinitiators 4
3.3 The mercury arc lamp 6
3.4 Light-Emitting Diodes (LEDs) 7
3.4.1 Design of optoelectronics and device physics 7
3.4.2 Electrical and optical properties 8
3.4.3 Spectroradiometer and radiometric quantities 9
3.5 Relative acrylate conversion by ATR-FTIR analysis 11
3.6 Micro-hardness measurement 11
4. Experimental 12
4.1 Diagnostic test of LED chips 12
4.2 Initial curing tests 13
4.3 Application and sampling 13
4.4 Analysis technique procedures 14
4.5 Examination of commercial products 14
4.6 Materials 14
4.6.1 Curing settings 15
5. Results and discussion 16
5.1 Diagnostic test of LED chips 16
5.2 Evaluation of analysis techniques 19
5.3 Analysis of commercial UV products 23
5.3.1 Pigmented top-coat 24
5.3.2 Pigmented base-coat 25
5.3.3 Clear top-coat 27
5.4. Multivariate analysis 29
5.5 Summary 31
6. Conclusions 32

7. Future outlooks 33
Acknowledgements 34
References 35
Appendix 1 37
Appendix 2 44
Appendix 3 45
Appendix 3.1 53
Appendix 4 54
Appendix 5 54

1. Introduction

Ultraviolet (UV)-curing acrylate systems is the technology of choice in modern high-speed wood coating lines, where instant curing and handling is required. The curing process is a fast (milliseconds) free-radical polymerization process initiated by the excitation of a photo initiating molecule by UV radiation. The mercury arc lamp is the conventional UV-source, used today which emits a wide range of output intensity lines in the UV and near visible spectrum (UVV) 200–450 nm with a power output of 180 W/cm^2.[1] However, the United Nations Minamata convention states that the conventional mercury-doped arc lamps used in the furniture and flooring coating industry today must be exchanged by mercury-free alternatives in the near future.[2] Mercury-free radiation sources that are used today are electron-beam, excimer lamps, light emitting diodes (LEDs) and complementary devices such as flash lamps and lasers.[1,3,4]

LEDs providing discrete wavelengths at 365 nm, 395 nm and 405 nm have been on the market for a while but shorter wavelengths in the UVC and UVB region (200–320 nm) have not been available until quite recently.[1] Building on a patent from Professor Amano Akasaki, awarded Nobel prize winner in physics (2014)[5], Japanese company Nikkiso released the same year UV-light emitting diodes generating short-wavelength (UVB and UVC), high-energy, electromagnetic radiation without the use of mercury. Benefits with the LED curing technique are the high-power conversion of injection current to UV light (efficiency), compared to a mercury arc lamp and that they generate essentially no heat and can be considered as "cold-cure" source.[1,6]

2. Objective

In this master project, it was examined if combinations of UVC, UVB and UVA radiation from UV-LEDs could be used as a source for curing acrylate coating systems and be a realistic, mercury-free replacement, of the mercury arc lamp in the future.

Seven LEDs from Nikkiso Co, ranging from 260–320 nm formed the basis of this study. The radiation output was characterized in radiometric quantities i.e., irradiance and dose that was monitored in a spectroradiometer. Microhardness indention test and Attenuated Total Reflectance-Fourier Transform Infrared (ATR-FTIR) was extensively used to analyze cured UV-coatings. The main objective for this project were:

- Comparing radiometric quantities with the conventional mercury arc lamp and correlate that to film forming properties after illumination.

- Screen various parameters in chemical formula composition and radiation output to connect the most important issues of successfully cure UV-paint and lacquers with short wavelength LED.

3. Theory

3.1 Complexity of UV paint formulations

The complexity of paints lies in their sophisticated formulations. Formulations of UV-paint can be divided into six main parts: (1) binders (oligomers), (2) monomers, (3) pigments, (4) extenders, (5) silica and (6) additives. Binders constitute the main bulk material in a paint. It adheres to the substrate and in the curing process forms a continuous film. The structure of the backbone will have an impact on flexibility, adhesion, and chemical resistance. Common backbone structures are epoxy, polyester, urethane and amino-modified oligomers. Polyfunctional oligomers contribute to high rates of cross-linking, and in combination with backbone structure, affects the main properties of the final coating. Monomers dilutes binders to a viscosity fit for application. In UV formulations nothing evaporates but rather form junctions, hence monomers are also called reactive diluents. Multifunctional monomers do increase the rate of cross-linking compared to a monofunctional monomer due to higher concentration of double bonds and the increased reactivity of pendant bonds and very hard coatings can be formed.[7,8] Presumably, low molecular weight (M_w) monomers can be packed denser as an effect of free volume availability (low volume exclusion) and has a high diffusion coefficient (D_t) which can be related to the hydrodynamic radius, R_h and the "solvent" viscosity, η_s.

$$D_t \equiv \frac{kT}{6\pi\eta_s R_h} \qquad (1)$$

Where $D_t \sim M^{-3/5}$ in a very good solvent.[9] The free volume decreases drastically as T_g is increased during polymerization and reaches the curing temperature T_{cure}. When T_g is equal to T_{cure} or just above, the curing rate is slowed down considerably. In general, backbone flexibility increases as T_g decreases. For achieving a high extent of acrylate group conversion, flexible, low-T_g coatings are preferred.[7]

Pigments set the color and opacity of the paint. Rutile titanium dioxide is the base of many pigmented formulations since it has very high reflective index in the visible spectrum (400–700 nm). Furthermore, various organic, and inorganic pigments are used for setting the right color. Chalk ($CaCO_3$) is a typical extender, and it is mostly used to extend the paint thereby keeping down the cost per volume unit produced paint, but also to adjust rheology. Extenders can also be used in primers to improve sand-ability.

Silica and fumed silica are mainly used as matting agents or to increase viscosity. They come with a variety of pore sizes and different wax surface treatments. Additives are various agents that can optimize paint properties such as defoamers, rheology agents, and wetting agents etc.

The main market for coating solutions of UV-paint is in the wood substrate section directed to furniture and flooring. There are high demands on quality and many criteria need to be fulfilled, such as surface finish, adhesion, reactivity, wetting ability, structure, chemical resistance, wear resistance, gloss, color, abrasion, hardness, and scratch resistance.

3.2 Principles of ultraviolet initiation of curing

Free-radical polymerization and cationic curing are the two chemical processes that are used in UV curing.[1,10] The former principle is the most common method concerning commercial applications, thus also extensively used at Sherwin–Williams where acrylate polymers are combined and polymerized.

The generation of free radicals (P·) occur by light absorption of photoinitiators (P) that are designed molecule structures that absorb in the UV region, between 200–420 nm. A high energy singlet (S_1) state is formed at sufficient energy which in turn can lead to radical production, either by intersystem crossing from singlet to triplet state (T_3) forming stable but less energetic radicals or directly from the singlet state (Figure 1). Triplet state free radicals are produced by most commercial photoinitiators. The main general decay processes like fluorescence (S_o) and phosphorescence (T_o) may occur from the respective state but also deactivating processes like quenching by oxygen or monomers.[1]

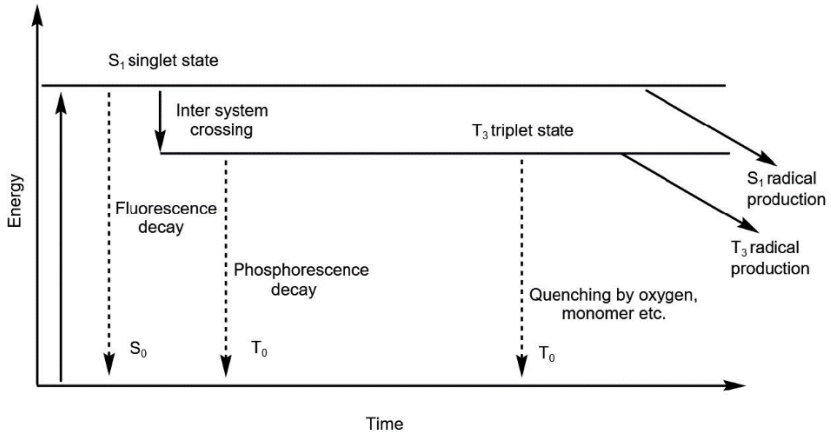

Figure 1. Jablonski diagram of the light absorbing process of photoinitiators.

Generation of free radicals and the rate of initiation of free-radical polymerization is highly dependent of the absorbance ability by a photoinitiator. Both surface and bulk curing must occur in the film formation, hence photoinitiators are designed to absorb at different energies due to the correlation between wavelength and penetration depth of the incident light. A photoinitiator can display one or several absorbance peaks in the UV range where the conversion of UV light to free radicals at different depths is highly efficient.[1,7]

3.2.1 Free-radical chain polymerization

The polymerization process involves four steps: (*1*) initiation, (*2*) propagation, (*3*) chain transfer, and (*4*) termination. Initiation has partially been outlined above, concerning the photoinitiators, UV absorbance and the formation of free radicals. The initiation step also comprises the reaction of acrylate functional groups (acrylic ester) with radical species, forming an active alkyl radical monomer according to the following reaction in Figure 2:[1,10]

$$R(\text{initiator}) + h\upsilon \rightarrow R\cdot(\text{radical})$$

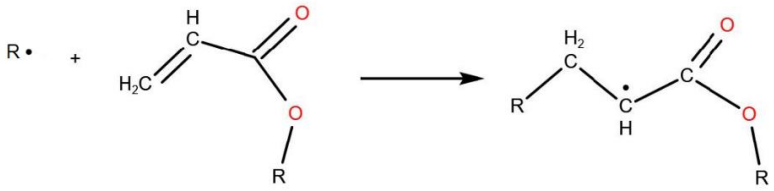

Figure 2. Initiation step of acrylate free-radical polymerization.

In the propagation step (Figure 3), the alkyl radical starts a chain reaction with another monomer/oligomer and keeps propagate, hence radical chain polymerization. If multi-functional acrylates are available, cross-linking structures occur, forming a polymer matrix.[1,7]

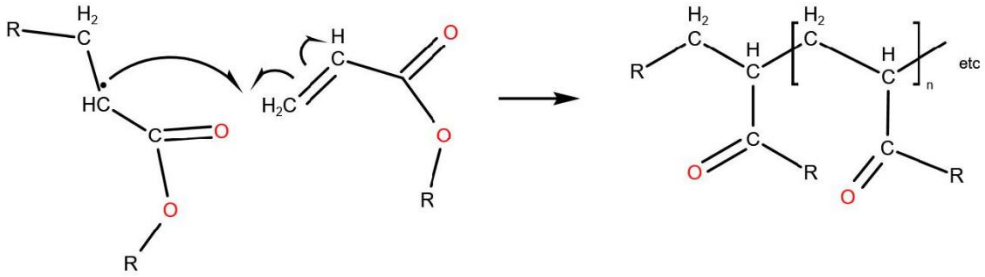

Figure 3. Propagation step of acrylate free-radical polymerization.

Chain transfer can occur when a hydrogen donor is introduced to the growing polymer radical. The growth of the polymer chain ends upon receiving a hydrogen, but the donor molecule becomes a donor radical which could interact with a new monomer with subsequent chain growth of a polymer. Hydrogen donors act as chain growth modifiers since they can reduce the average M_w due to the chain transfer process. They are also necessary in the type II initiation process which will be discussed in the next section. Chain termination can occur by mechanisms such as recombination or disproportionation, resulting in a neutral species and the growth of the polymer chain is stopped.[1]

The rate and efficiency of the free-radical chain polymerization depends on many factors. Initiation is the only photosensitive step thus dependent on type of photoinitiator combined with irradiance and dose, i.e., the radiant output from the UV source. The subsequent free-radical polymerization is thermally driven, and the curing process is influenced by the formulation: monomers, binders, pigments, and additives will give different properties like functionality, light scattering effects, hydrogen donors, viscosity, and light absorption.[1,7]

3.2.2 Photoinitiators

The chromophore that is most efficient in forming free radicals is the aryl ketone group shown in Figure 4. The mechanism by which free radicals are formed, a Type I scission or Type II abstraction process, depends on the

type of substitution groups that are attached to the ketone at R_1. An alkyl group at R_1 leads to a Type I scission process while a substituted aryl group at R_1 will provide a Type II abstraction process.[1]

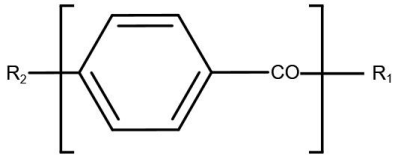

Figure 4. Aryl ketone group.

Substitution at R_2 will influence the absorption wavelength of the photoinitiator for both Type I and Type II. Groups with an enhanced electron donation feature will red-shift the absorption of the photoinitiator to longer wavelengths. UV radiation can provide around 70–80 kcal/mol energy output that is enough to cleave the CO-alkyl (R_1) bond (65–70 kcal/mol) for a Type I photoinitiator which results into two free radicals from an excited triplet state. An example is shown for a common hydroxy-acetophenone in Figure 5.[1]

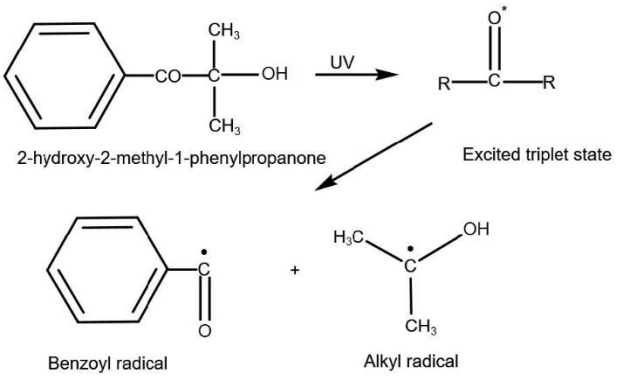

Figure 5. The Type I scission process.

For a Type II photoinitiator with an aryl-conjugated group at R_1, the bond energy for the CO–aryl bond is slightly higher but enough to prevent cleavage at that bond. The photoinitiator will absorb the available UV radiation but remains in an excited triplet state until it is approached by a hydrogen donor e.g., tertiary esters, ethers, amines etc., that is equipped with an activated hydrogen (α-atom) next to a hetero atom. Upon receiving a hydrogen, the

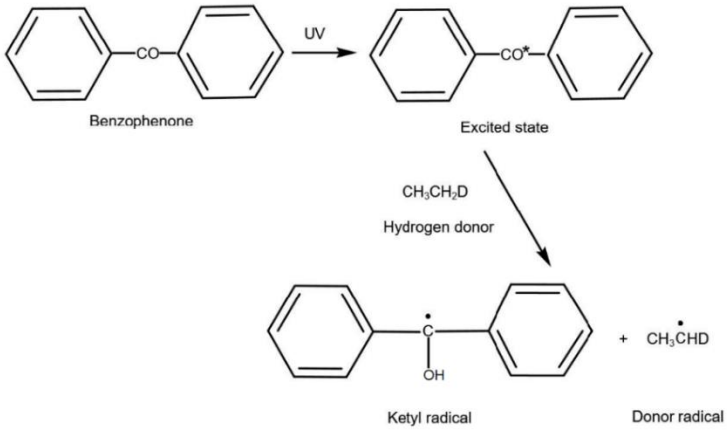

Figure 6. The Type II abstraction process.

excited

triplet state is producing a ketyl radical with low reactivity and a donor radical with high reactivity, see Figure 6.[1]

The rate of scission of a Type I photoinitiator is generally increased by electron-donating groups at R_3 which leads to a higher photoactivity (Figure 7a). For a Type II photoinitiator, electron donating substitution on either aryl-conjugated ring gives similar rise of red-shift and higher photoactivity, since its structure is equal around the CO bond (Figure 7b). Electron-withdrawing substitution hence have a negative effect on the photoactivity of both Type I and Type II photoinitiators.[1]

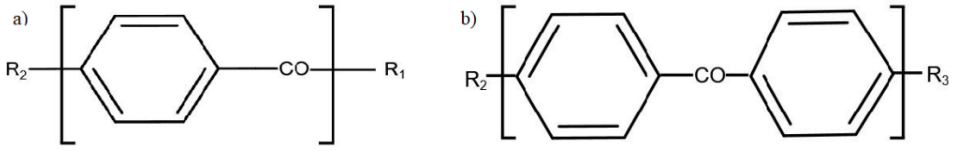

Figure 7. a) Alkyl aryl ketone (Type I) and b) aryl ketone (Type II).

3.3 The mercury arc lamp

The mercury arc lamp has been used since the inception of the UV curing industry. It is generally composed by a sealed quartz tube with two electrodes at each end made of tungsten that are connected to an electric source. The quartz tube contains a specific amount of mercury and starter gas, usually argon. The starter gas is easily ionized and enables current to flow that allows the lamp to heat up to its operating temperature (600–800 °C), at these temperatures, all the mercury is fully ionized, and a stable, high voltage arc is struck that activates the mercury lamp. The mercury vapor provides one atmosphere pressure and is excited by the high-voltage arc to several higher energy levels. These excited states are unstable, and the atoms are relaxed to their ground state. Energy is released during the relaxation process and produces a wide range of emission lines throughout the UV spectrum but also a significant part of visible and infrared light. The main emission lines are at 253nm, 313 nm, 366 nm, 404 nm, and 436 nm. Figure 8 shows the output distribution of the mercury arc lamp used in this study. Most commercial photoinitiators absorb at one or several of these intensity lines and initiate free-radical polymerization.[1]

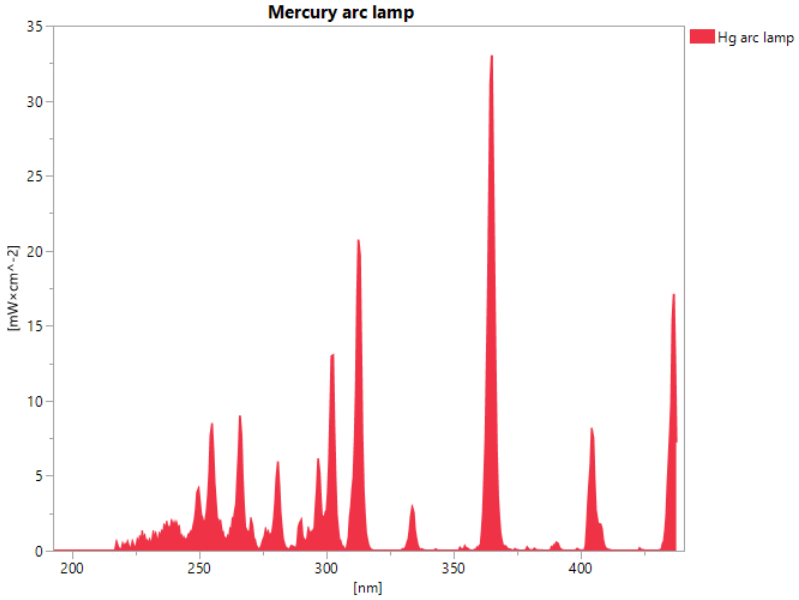

Figure 8. Typical spectrum of intensity output lines by the mercury arc lamp.

3.4 Light-Emitting Diodes (LEDs)

Semiconductor light sources in the form of light emitting diodes in the UVC spectral range were successfully developed in the early 90s by two independent research groups, Isamu Akasaki and Hiroshi Amano at Nagoya University and Shuji Nakamura who was employed at Nichia chemicals, a small company in the city of Tokushima, Shikoku.[5] LEDs are p-n junction devices that consists of a solid-state double heterostructure, forming two-electrode semiconductors that convert electrical energy into light (Figure 9a). A p-n junction diode must be forward-biased, i.e., the current can only be driven one way. Specifically, the forward-biased current direction (by convention) goes from the anode (+) to the cathode (-) even though the free electrons (n) moving from the n-layer to the p-layers are carrying the actual electric current.[6] Holes (p) are moving the opposite way to the free electrons and in the active region, they are contained in a multiple quantum well structure (MQW) where holes and free electrons recombine and light is emitted.[5] Figure 9b show the same general LED double heterostructure in more detail.

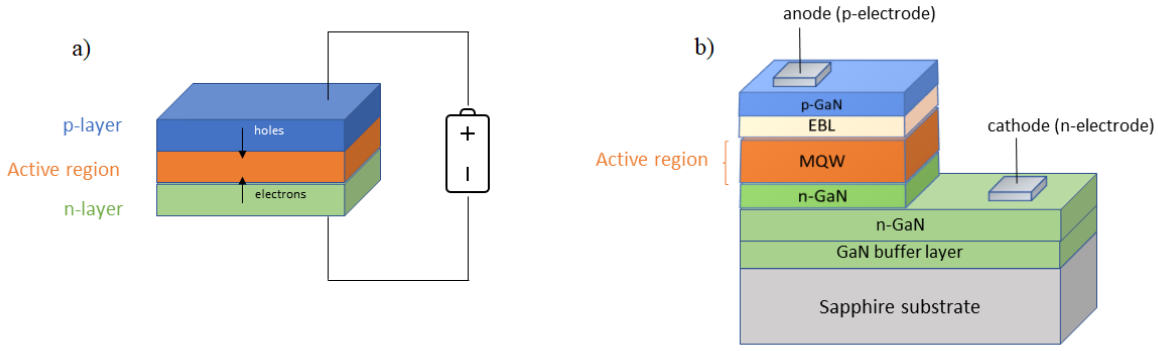

Figure 9. General device structure over a LED chip with n- and p-dopant layers (a) and a more detailed construction of the same LED double heterostructure (b) with electron blocking layer (EBL), multiple quantum wells, sapphire substrate and the composition of p and n-layer.

Both competing projects were successful in growing Gallium nitride (GaN) crystals on sapphire (α-Al_2O_3) wafers in slightly different ways, hence all three received the physics Nobel price anno 2014.[5] Sapphire substrates are convenient for epitaxial growth and LED functionality due to high hardness, thermal stability, and it is transparent in the visible spectrum. Substrates of sapphire are also suitable for mass production because of readily attained high crystallinity combined with cheap production cost. Disadvantages are the big mismatch in lattice size which deteriorates the possibility of direct band gaps and the difference in thermal stability coefficient which causes thermal stress leading to dislocations and cracking.[11] Akasaki and Amano solved the lattice mismatch by exposing the sapphire surface to Nitrogen and built thin layers of aluminium nitride (AlN) which worked as an intermediate, lattice-matched layer between the substrate and GaN epilayers, reducing the lattice mismatch from 14% to 3%. Shuji Nakamura used strained-layer epitaxy by building thin layers of GaN on the sapphire substrate followed by thicker layers of GaN.[5]

3.4.1 Design of optoelectronics and device physics

The optoelectrical design of semiconductors has been extensively improved during the last two decades. Heterostructure lattice-matched layers, strained layer epitaxy, and multi-quantum well design are still the key parameters in designing LEDs by tuning their band gaps and power output.[12] This subsection will briefly go into a deeper understanding in LED design and correlate that to the emitting magnitude of dose [$mJ \times cm^{-2}$] and irradiance [$mW \times cm^{-2}$] which are of great interest in UV-curing systems.[13]

When a p-doped and an n-doped material with different fermi levels (E_F) are combined, forming a junction, a diffusion process begins of charge carriers (holes and electrons) due to the difference in charge carrier

concentration. An active region of electrons and holes forms at the junction to a certain degree until thermal equilibrium is reached. The fermi level is independent of this diffusion process and remains constant in the active region. The typical appearance of band bending shown in Figure 10 occurs by the charge migration and results in a potential energy gradient through the active region. A typical design of a quantum well structure by arbitrary composition and layer thickness is shown as well.[14]

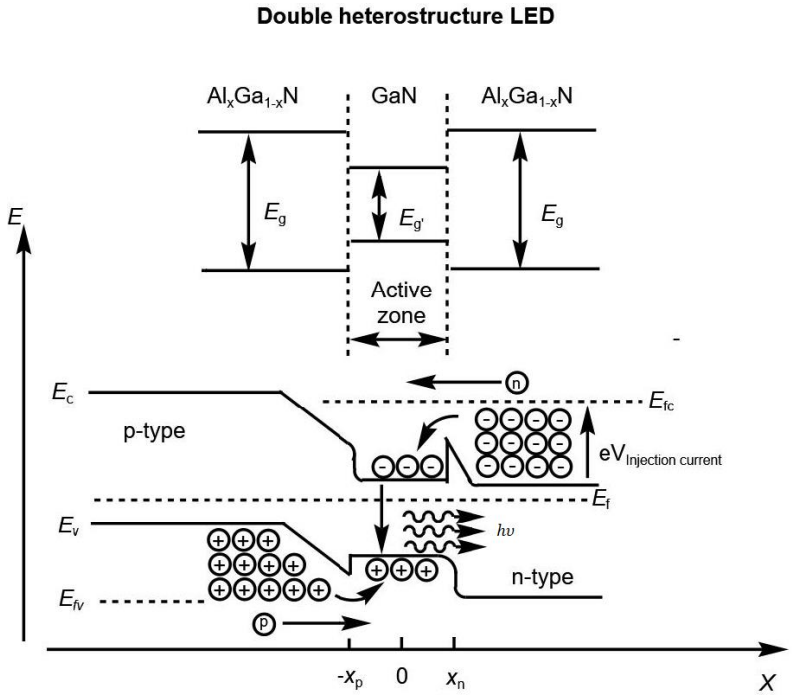

Figure 10. General design of a LED double heterostructure with an arbitrary amount of aluminium dopant, constructing a quantum well by band gap (E_g) engineering. Injection current (eV) leads to quasi fermi levels (E_{fc}) and the LED is forward-biased.

If an external biased injection current is applied according to figure 10, charge carriers are injected into the active region. Injected electrons that flow into the n-doped material will raise the energy potential correspondingly to the p-type material due to the destabilizing effect of electron injection. The increased energy potential of the valence and conduction band in the n-doped material leads to the state of quasi fermi levels (E_{fc}, E_{fv}) which independently describe the concentration of electrons and holes in the active region. Due to the rise in energy potential, electrons (n) and holes (p) can overcome the designed energy barrier and freely flow into the active region where they are confined by the quantum well structure. The carrier concentration in the active region is highly increased and the number of recombinations in the active region, hence emissions per unit volume in the active region will increase as well.[15,16]

3.4.2 Electrical and optical properties

As previously explained, LEDs are forward-biased, and the magnitude of the photoemission is a function of the applied forward voltage (V_F) and forward current (I_F). Constant electrical current is highly recommended to use since the radiant flux (power output) is highly dependent of the applied current. It is also important to control the current due to the high temperature dependence. If too high current densities are driven through the p-n junction, defects to the crystal structure can arise due to thermal expansion and the recombination process is locally disturbed, so called “dark line effects” and photons cease being emitted. If even higher levels of heat generation occur in the diode it could lead to fatal rupture and breakage of the LED.[6] The power output (radiant flux) is the main characteristic that the describe the quality of the LED chip. It is assessed by Equation 2.[17]

$$P_{\text{out}} = \eta_{\text{ext}}(i/e)h\upsilon \quad (2)$$

$$P_{out} \propto i \quad (3)$$

The external quantum efficiency (η_{ext}) which is a product of internal quantum efficiency (η_{i}) that is mainly dependent on material properties, and extraction quantum efficiency (η_{e}) that is dependent by the device structure quality.[17] The linear dependence of power output is stable to a maximum value of injection current. If the injection current is continuously increased over the maximal value, saturation and lowering of the radiation output will occur by increased internal diode resistance (Joule heating) which will increase the rate of non-radiative recombinations by phonons due to increased lattice vibration.[6]

3.4.3 Spectroradiometer and radiometric quantities

The conventional method of measuring irradiance and dose in the UV-coating industry is to use a radiometer. Radiometers are suited for broadband spectra as originated from mercury arc lamps. They have sensors with broad and non-symmetrical spectral response over a fixed range, such as UVA, UVB or UVC and are calibrated to one lamp type. These features make a radiometer unfit for measuring the radiation emitted from an LED since their spectral output has a narrow bandwidth in the range of 20–50 nm.[18,19] The radiometer used at Sherwin–Williams is Power Map® by EIT whose bandwidth response is shown in Figure 11. There is a sensitivity drop in range 260–280 nm with a minimum at 270 nm, as well as around 320 nm which will lead to measurement errors for semi-discrete wavelengths in that range.

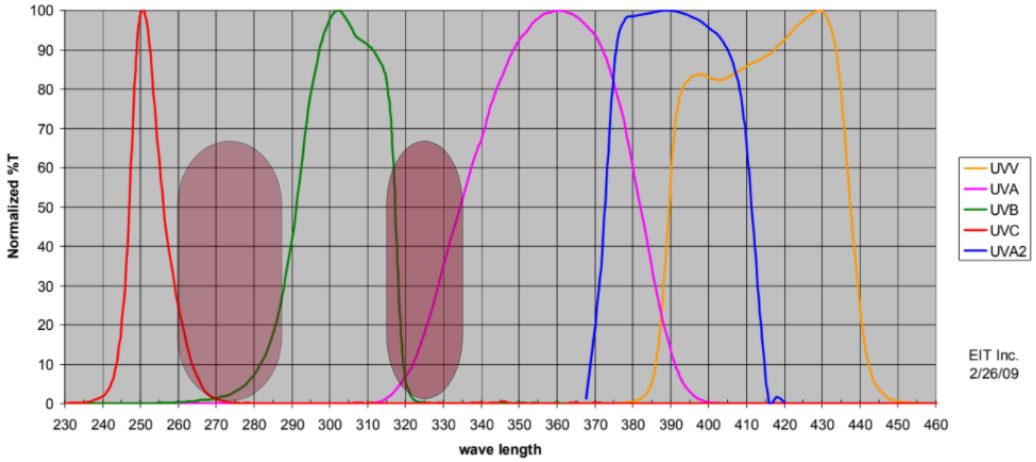

Figure 11. The spectral transmittance (T), (UVV, UVA, UVB, UVC, and UVA2 filters) of the Power map® radiometer used at Sherwin–Williams, with highlighted sensitivity drop in red.

Spectroradiometers can measure the radiant energy for any type of light-emitting source. By the means of prisms or photodiodes, polychromatic light can be divided into monochromatic light where each constituent component is measured. The data output from a spectroradiometer are radiometric quantities presented in energy units.[18]

Explanations of radiometric quantities and their terminology:[6]

- The *radiant flux*, ϕ or radiant power which it is also commonly termed, is the transfer rate of radiant energy, θ from a radiant field to another region e.g., emission of a photon from LED chip to an arbitrary surface. Radiant flux is denoted $d\theta/dt$ and has unit in watt [W].

- The *radiant intensity* is the radiant flux per unit solid angle, Ω emitted from a light source at a fixed distance, *r*, in a given direction, denoted $d\phi/d\Omega$ and has the unit of watts per steradian, [$W \times sr^{-1}$]. The solid angle, Ω is unitless and is given by $\Omega = A/r$, where A is the illuminated spherical area from a point source at a given distance, *r*.

- *Irradiance*, *E* is the incident radiant flux at a surface per unit area, denoted $d\phi/dA$ and has the unit of [$W \times m^{-2}$]. The Irradiance is also denoted *flux density* in some literature but, also commonly referred to as *peak* in the UV-coating industry.

- *Dose* is the irradiance integrated over time, denoted *dE/dt* in the unit of [$J \times m^{-2}$].

The total irradiance and dose are the key outputs that are given by a spectroradiometer in single numbers. The irradiance is also given for every discrete wavelength within the light source bandwidth in iterative steps with unit of [$(mW \times cm^{-2}) \times nm^{-1}$]. Irradiance is governed by the inverse-square law (Equation 4) under the conditions of being a point source.[6]

$$E = \frac{I}{d^2} \tag{4}$$

where *I* is the radiant intensity and *d* is the distance from the origin of the light source to the detector. The light source needs to strictly be considered as a point source and the surface needs to be perpendicular to the direction of the incident light. LEDs are not point sources hence the cosine law needs to be applied for the angular distribution of the incident light and the rotational symmetry of the LED which can be approximated by[6]

$$I(\theta) = I_0 \times cos^{\mathrm{m-1}}\theta \tag{5}$$

where m = 1, 2, 3….

The constant *m* is a geometric constant for the light source which is individual and dependent on both material and structure designs.[6]

Another important aspect to recognize is that dose is time-dependent whilst irradiance is not. In practical measurements of power output, the applied belt speed in an industrial coating line will affect the dose but not the irradiance.

3.5 Relative acrylate conversion by ATR-FTIR analysis

FTIR is a valuable and very precise fingerprint technique to identify, characterize and quantify a wide range of solids, liquids, and gases. In traditional measuring methods by FTIR, radiation in the IR range is transmitted through the sample where the interaction with the sample is detected in form of absorbance, transmittance, or reflectance. This procedure limits the sample thickness for solids and liquids which cannot be larger than a few hundred nanometers. The spectral intensity of all detected features is also thickness-dependent. Rigorous sample preparation is needed for solids. In general, a solid is grinded to a fine powder and dispersed into a liquid forming a homogenous paste which is uniformly spread between two infrared-transparent windows. Since this type of sample preparation is very sensitive to matrix ratios and homogeneity, large variance and standard errors is expected between measurements that will lead to poor spectral reproducibility.[20,21]

Attenuated Total Reflectance (ATR) addresses the issue of poor reproducibility. An incident infrared beam at a crystal with high refractive index (ZnSe, Ge, Pt-diamond) generates an internally reflected beam which in turn creates an evanescent wave that can extend beyond the crystal and will interact with an applied sample, i.e., becomes attenuated. The altered waves are reflected back at the IR beam and can consequently escape at the opposite end of the crystal thereby being directed to the detector. This procedure is shown in Figure 12. Two distinct requirements for successful measurements need to be obliged for this technique to work properly. First, the sample needs to be in good contact with the crystal due to the low order of extension by the evanescent wave into the sample (0.5–5 µm). Second, the ATR crystal must have a significantly greater refractive index than the sample for the IR beam to be internally reflected in the crystal instead of being transmitted.[20,21]

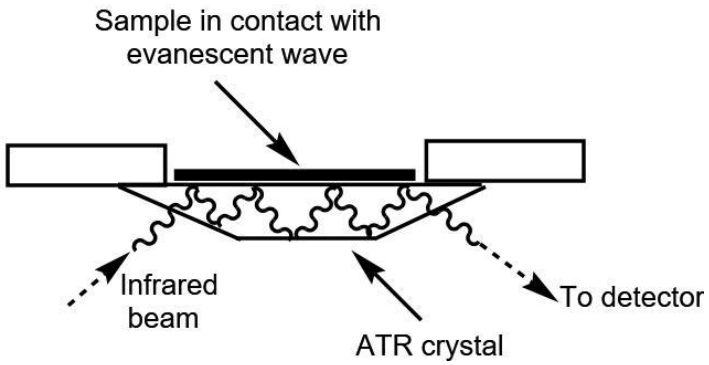

Figure 12. The process of ATR sampling where an evanescent wave interacts with a sample.

It has been shown that ATR-FTIR is a robust method for relative quantification of cross-linking density in various polymeric structures with a low relative standard deviation.[22,23] Acrylate-based formulations have characteristic absorption bands that arise due to C=C double bonds at 810 cm^{-1} (out-of-plane deformation vibration), and at 1407 cm^{-1} (in-plane deformation vibration), respectively.[24] The C=C bond is opened and consumed during the initiation step as previously explained. By implementing a two-point calibration where two samples from the same batch are measured with ATR-FTIR, where one sample is exposed to an excess of UV light (fully cured) whereas the other sample is not exposed at all (wet sample), a relative quantification of the extent of acrylate conversion can be performed for a third sample (same batch) that is exposed to an arbitrary output of UV radiation. Relative quantification is monitored by integrating acrylate peak intensities and calculating the ratio between the wet sample and a cured sample.

3.6 Micro-hardness measurement

Hardness test by micro-indentation is performed by either Vickers or Knoop test. The indentation depth h is characteristically of $h > 0.2$ µm and the applied load L is no larger than $L > 2000$ mN. The resistance of the coating

layer is correlated to the time-dependent penetration depth of a diamond indenter under a given load with a certain geometry (pyramid). Hardness is calculated in "Martens Hardness" (HM) units of N×mm^{-2} by ISO 15477 for symmetric pyramidal indenters like Vickers and Berkovich where the apex angle is 136°. The area of the substrate, A_s as a function of penetration depth gives:[25]

$$A_s(h) = \frac{4\sin(\alpha/2)}{\cos^2(\alpha/2)}h^2 = 26.43h^2 \quad (6)$$

and the HM is given by:

$$HM = \frac{L_{max}}{A_s(h)} = \frac{L_{max}}{26.43h^2} \quad (7)$$

As h increases, the substrate will contribute additionally to the calculated HM of the applied coating due to its mechanical properties. Bückle's "rule of thumb" states that h must not be more than 10% of the coating thickness to avoid any contribution. However, the rule is flexible and ratios of yield strength (σ_y) and Young's Modulus (E) between coating and substrate will affect the indentation response. It has been found that Bückles rule is only applicable if $\sigma_{yc}/\sigma_{ys} < 10$ and $E_c/E_s > 0.1$ but in cases where the coating is very soft (HM < 0.5 GPa) on a hard substrate (HM > 10 GPa), the substrate deformation will not influence the indentation response even at an indentation depth that is 50% of the film thickness.[25]

4. Experimental

4.1 Diagnostic test of LED chips

Seven LEDs from Nikkiso with peak emission wavelengths (λ_p) in the range of 260–320 nm were connected to a pre-installed junction box, one for each chip. The output performance for every LED chip was monitored by directing it at a detector window of a spectroradiometer, (UVpad by Opsytec Dr. Gröbel) while forward-biasing. The radiation was directed at a constant angle, perpendicular to the optical active surface with a constant distance (d) of 5.3± 0.1 mm for 24 s. Iterative measurements were performed for each LED at a fixed integration time for reproducible results. Additional measurements were made and monitored with the UVpad performing the same procedure but at longer fixed distances, d = 6.9, 8.6, 11.9, 15.2, and 18.5 ± 0.1 mm. All distances were set by either distance blocks by 3.3 mm or by four screws that were leveled in each corner of the junction box and measured with a digital caliper. The diodes were forward-biased with a constant-current DC power supply, (RND lab 320-KD3005D). Single-value data of irradiance [mW×cm^{-2}] and dose [mJ×cm^{-2}] (total, UVA, UVB, and UVC) was achieved for every measurement. The absorbance peak spectrum [(mWcm^{-2})×nm^{-1}] with additional data table was also collected. Data was also collected from the lab mercury arc lamp (TRIAB) at different distances, power outputs and belt speeds.

4.2 Initial curing tests

The LED with peak emission wavelength of 280.0 nm was chosen to perform as radiation source in the initial curing tests due to reasonably high radiant flux at the shortest emission wavelength.

To evaluate if curing was possible at all with the LEDs, a basic but very reactive test formulation (S1) was mixed, containing amino-modified binder, linear diacrylate monomer combined with benzophenone and phosphine oxide photoinitiator. The purpose by this initial stage of experiment was also to evaluate Micro-Hardness and ATR-FTIR as analysis techniques by measuring cured samples of S1 and analyze the data response.

4.3 Application and sampling

Wet sample (S1) was applied on a transparent glass substrate, 220×100×30 mm with a 4-sided applicator frame, (Zehntner ZAF 2010 S/N52426010). The applicator thickness was 20 µm and the sample was thermostated to 23 °C. All applications within this project were performed accordingly and are here after considered to be a standard procedure throughout this report.

Curing was performed with the same procedure as that of the LED diagnostic test. The resulting cured areas had the geometry of a "squircle" or truncated circle, see Figure 13. Cured areas varied with time of illumination, i.e., dose and with distance, i.e., irradiance between the LED chip and applied coating. Curing was also performed with the mercury arc lamp at an excess of UV light and at doses according to the quality control (QC), control plan for a specific product as a reference for conventional curing.

The LED is expected to have an angular distribution of light, hence a curing gradient from the center to the edge of the cured area was expected due to the radiant intensity cosine dependency of the solid angle to a given distance. All data was collected on the cured sample within an area no larger than the area of the optically active surface of the UVpad. This implementation was introduced to verify that the same amount of radiation had exposed all analyzed surfaces equivalently and could be quantified with collected UVpad data. The optically active surface at the UVpad had a diameter of 6.0 mm and a calculated area of ~0.28 cm^2.

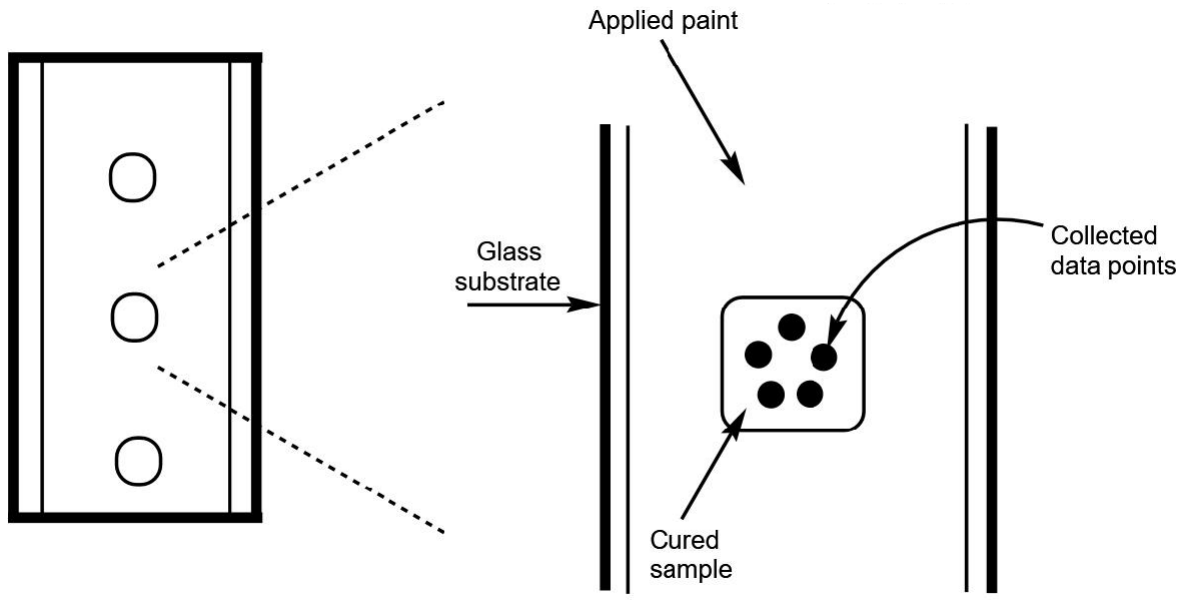

Figure 13. Example of application on glass substrate, LED-cured sample and how sampling was performed.

4.4 Analysis technique procedures

Micro-hardness measurements of cured coating samples were applied with a Fischerscope H-100, (Fischer Instrumentation). The indentation load was set to 100 mN/20 s. The yield strength, σ_y and Young's modulus, E are assumed to follow $\sigma_{yc}/\sigma_{ys} < 10$ and $E_c/E_s > 0.1$, hence Bückle's law applies and the indentation depth, h, should not exceed more than 10% of the film thickness. A number of 2–5 individual data points was collected for each sample, depending on what the cured samples area allowed. Hardness measurement data was monitored with associated software. Hardness is presented in Martens Hardness (HM) with the unit [$N \times mm^{-2}$].

Quantification of the relative extent of acrylate conversion was calculated by measuring cured films in an ATR-FTIR (diamond crystal) spectrometer, (Bruker optic, Tensor 27) and then integrating relative transmittance peaks at 810 cm^{-1} and 1407 cm^{-1} with associated software OPUS (Optics User Software). A background measurement was acquired before every sample measurement. Baseline correction was performed by using "Rubberband correction" and 64 baseline points. A number of 3–5 data points was collected for each sample. For the initial test sample, S1, only data on the top of the film were collected. For subsequent tests, measurements from both the top and bottom of the film were collected.

The cured films had to be peeled off from the glass substrate in order to be in contact with the diamond crystal during measurement. Distilled water was used to separate the film from the substrate. Samples were then dried from remaining water on lab tissues protected by light-reflective foil. The ratio between the obtained integrated area of a cured sample over the integrated area of the wet sample was calculated and converted to the relative extent of conversion of acrylate groups [%].

4.5 Examination of commercial products

After sample S1 had been examined and both micro-hardness and ATR-FTIR were evaluated as analysis techniques, three established commercial products were evaluated in further experiments: One "clear top-coat", one "pigmented base-coat", and one "pigmented top-coat". Individually, they would represent a coating layer in a coating "sandwich layer" system, thus having widely separated properties and functions. These different features are a result of recipe formulation and some of them are highlighted in the materials section. A commercial 395 nm LED unit (Phoseon, Fire jet 220), containing 216 LED chips was introduced in this stage of the experiments due to that rutile TiO_2 pigmented formulations needs longer wavelength UV light (~420 nm) bulk cure. Here, all three products were individually exposed with one of the seven LED chips at a time, at various irradiance and dose. Pigmented base- and top-coat samples were additionally bulk cured with one passage under the 395 nm LED unit (108 $mJ \times cm^{-2}$).

4.6 Materials

The materials used and their ratios are given in Table 1 for the initial curing test of sample S1. Additional information is presented such as the main peak absorption lines by the photoinitiators and formulation viscosity.

Table 1. Composition and QC control plan of sample S1.

Mixture components	Type	wt%	UV absorption [nm]	Test method	Value	Unit
Binder	Amino-modified acrylate	80	-	Viscometry	1100	mPa×s
Monomer	diacrylate	15	-			
Photoinitiator	Benzophenone (type II)	3	251, 333			
Photoinitiator	Phosphine oxide (type I)	2	230, 275, 330			

The most important aspects of the formula composition by the three commercial products used in the subsequent experiments are presented in Table 2.

Table 2. Composition and QC control plan for the three commercial products. Photoinitiators with different index are of the same chemistry but are of different commercial products names and can deviate in their properties.

Materials & QC Control plan	**Clear top-coat**	**Pigmented base-coat**	**Pigmented top-coat**	**UV absorption [nm]**[26]
Binder(s)	Modified bisphenol A epoxy acrylate	Modified bisphenol A epoxy acrylate	modified bisphenol A epoxy acrylate	-
	-	Polyester acrylate	-	-
Functionality	2	2, 4	2	-
Monomer functionality	2,3	-	2	-
Pigments	-	TiO_2, 30 wt%	TiO_2, 11.4 wt%	-
Photoinitiators	Hydroxyacetophenone[1] (Type I)	Hydroxyacetophenone[2] (Type I)	Hydroxyacetophenone[1] (Type I)	(243, 280, 331)[1,2]
		Phosphine oxide[1] derivative (Type I)	Phosphine oxide[2] derivative (Type I)	(384)[1] (230, 275, 370)[2]
			Oligomeric alpha hydroxy ketone (Type I)	(260)
	Metylbenzoylformate (MBF Type I/Type II)	-	Metylbenzoylformate (MBF Type I/Type II)	(255, 325)
	-	-	Polymeric bezophenone derivative (Type II)	(240, 280, 330)
Viscosity[mPa×s**]**	990	11 200	1400	
Dose [mJ×cm^{-2}**]**	283	283	566	

4.6.1 Curing settings

Settings for 1 passage of curing with the conventional mercury arc lamp and the 395 nm LED unit which was used in the curing experiments is given in Table 3. The dose of 283 [mJ×cm^{-2}] correlates to 100 [mJ×cm^{-2}] in the UVB range measured by the Power Map® which is the conventional method at Sherwin–Williams.

Table 3. Curing settings for the mercury arc lamp and 395 nm LED unit.

Radiation source	**Power [%]**	**Height [mm]**	**Belt speed [m/min]**	**Irradiance [mW×cm^{-2}]**	**Dose [mJ×cm^{-2}]**
Mercury arc lamp (TRIAB)	17.7	150	27	1219	283
395 nm LED unit (Phoseon)	48.5	90	40	492	108

5. RESULTS AND DISCUSSION

5.1 Diagnostic test of LED chips

The product information that was co-sent with the LEDs is presented in in Table 4.

Table 4. LED chip inspection report.

Item	**Radiant flux (average)**	**Forward Current**	**Forward Voltage (average)**	**Peak Emission Wavelength (average)**
Symbol	ϕ	I_f	V_f	λ_p
Unit	[mW]	[mA]	[V]	[nm]
LED 260 nm	15.4	300	5.74	266.1
LED 270 nm	16.7	300	5.50	268.3
LED 280 nm	51.5	350	5.00	280.0
LED 290 nm	55.6	350	6.17	286.8
LED 300 nm	30.5	350	5.86	300.1
LED 310 nm	69.8	350	4.93	309.6
LED 320 nm	64.6	350	4.74	313.6

The irradiance [$mW \times cm^{-2}$], commonly referred to as peak in the UV coating industry, to distance dependence is shown in Figure 14 at d = 5.3, 6.9, 8.6, 11.9, 15.2, and 18.5 ± 0.1 mm for all seven LEDs. Complete table is attached in the appendix 1.

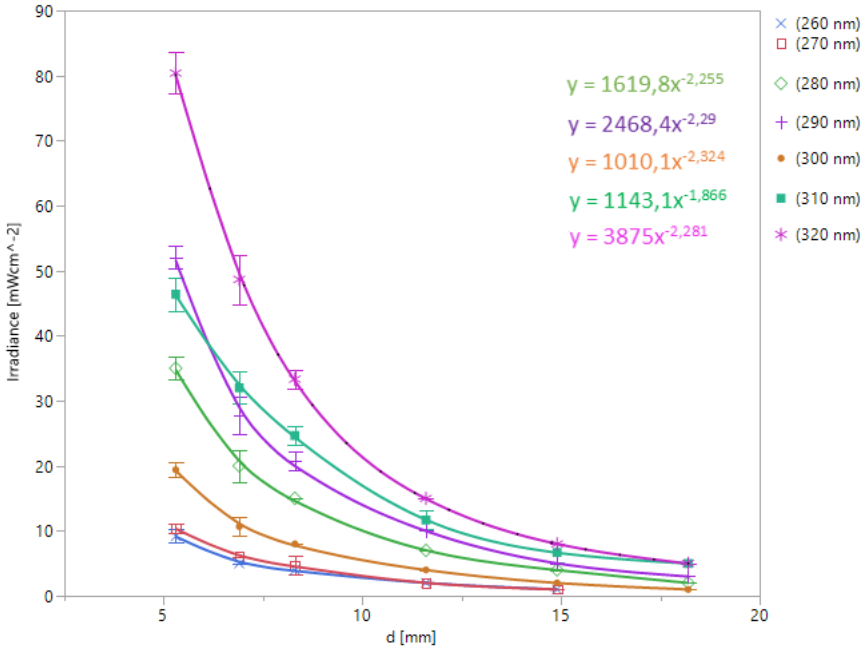

Figure 14. Irradiance (peak) measured at various distances.

The irradiance is characteristically decreasing with increasing distance between LED and detector. Drawing a smoothing spline fit (λ=0.01) through the mean value of data for each LED gives an inverse square equation in the form

$$E_n = Kd^{-x} \qquad (8)$$

where $K = I$ and $I_{280\ nm} \neq I_{290\ nm} \neq \ldots \neq I_{320\ nm}$ and x takes a value of 1.866 to 2.324. These equations should follow the inverse-square law (Eq. 3) so any deviation of x=2, can be considered as measurement error or that the distance from the LED chip to the detector window is too small and the LED is not acting as a point source. It was observed that the irradiance measured by the LED chips was well below the irradiance output of the mercury arc lamp (1219 mW×cm^{-2}) even at 5.3 mm. The irradiance can simply not be compared equivalently throughout these tests, but the dose can since it is time-dependent.

In Figure 15 the irradiance at 5.3 mm is compared to the average radiant flux [mW]. The irradiance is highly connected to the output values of the radiant flux. Trend wise, only LED 320 nm gives higher irradiance than its average radiant flux which indicates a narrower angular distribution of light emission due to higher radiant intensity at a constant area (detector window). The same reasoning applies for LED 290 nm which has a higher value of irradiance than 310 nm at 5.3 mm even though LED 310 nm has the highest radiant flux of all seven LEDs. With today's knowledge it is easier to maximise the external quantum efficiency (η_{ext}) for LEDs with longer emission wavelengths. This trend is contained from these results where only LED 300 nm obviously deviates, probably due to bad quality.

It is also important to notice that LEDs of 260 and 270 nm are only forward-biased at 300 mA compared to 350 mA for the others, where the current injection is directly proportional to the power output (Eq. 2). These material structures are probably more sensitive to joule heating than the other LEDs in the UVB spectral range.

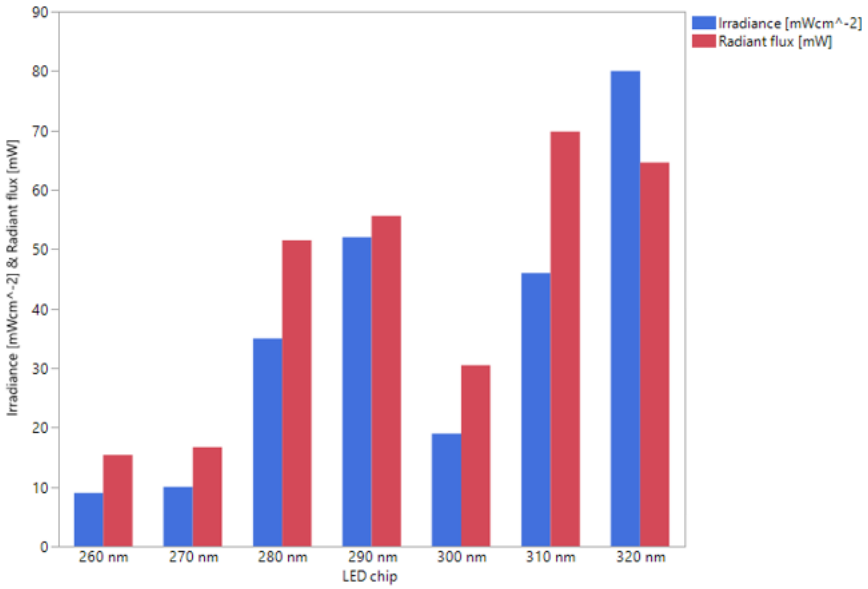

Figure 15. The correlation between the radiant flux and the measured irradiance at 5.3 mm for LED diodes with different wavelength.

Figure 16 shows the UV output intensity lines for the mercury arc lamp [1219 mW×cm^{-2}], the 395 nm LED unit [492 mW×cm^{-2}], and the 320 nm LED chip [80 mW×cm^{-2}], where the integrated area under each spectrum is the total irradiance output. As can be seen, LEDs produce a semi monochromatic output spectrum while the arc lamp produces a continuous output spectrum in the UV and near-UV range, with radiation from 215 nm to 420 nm and some distinct peaks typical for mercury-doped UV arc lamps.

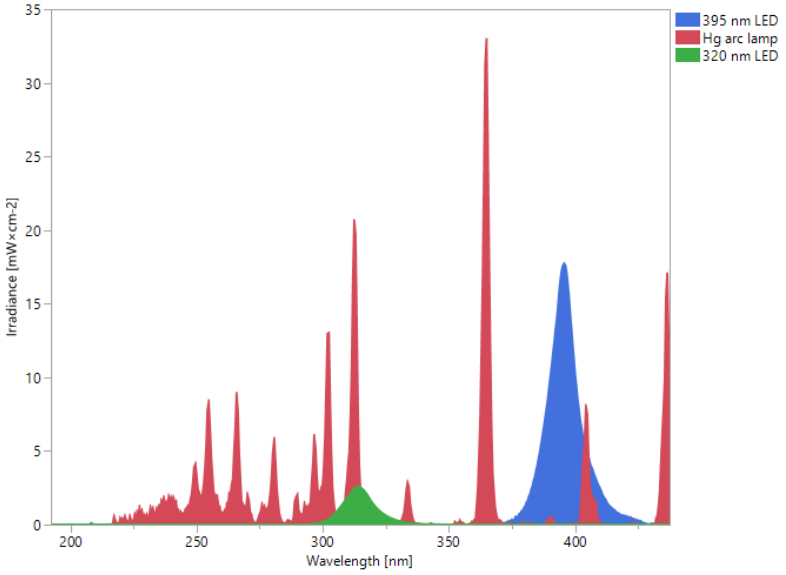

Figure 16. Spectrum of UV output intensity lines by the mercury arc lamp (red), 395 nm LED unit (blue), and the 320 nm LED chip (green).

5.2 Evaluation of analysis techniques

The ATR-FTIR spectrum for S1 as wet sample and excessively cured is shown in Figure 17.

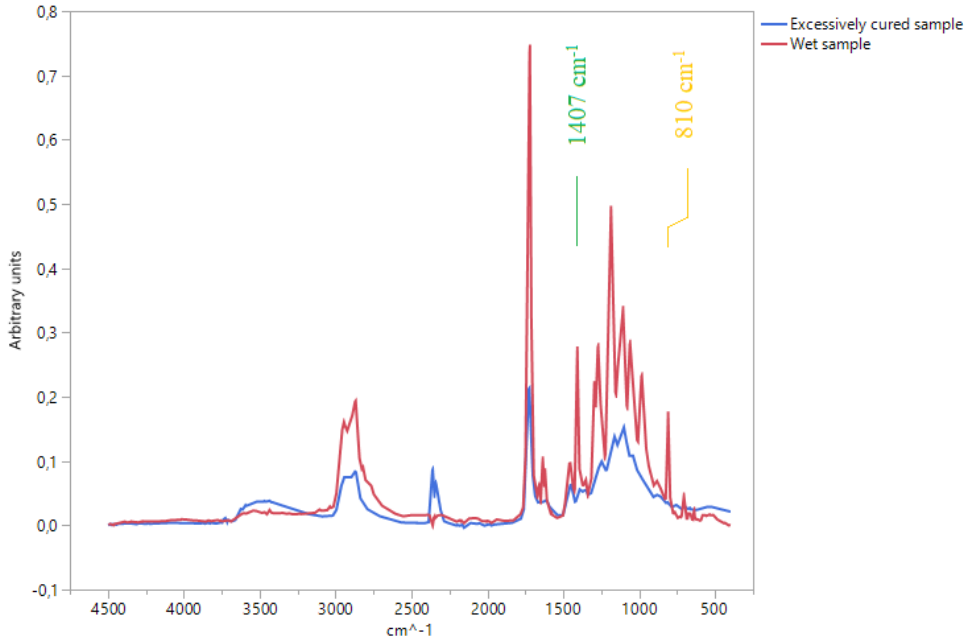

Figure 17. ATR FTIR spectrum over sample S1 as wet and excessively cured by the mercury arc lamp with peaks related to acrylate functionality indicated.

Resulting acrylate bands of intermediate curing with LED 280 nm at constant d = 5.3 mm are presented in Figure 18 and 19 at wavenumber 1407 cm^{-1} and 810 cm^{-1} respectively.

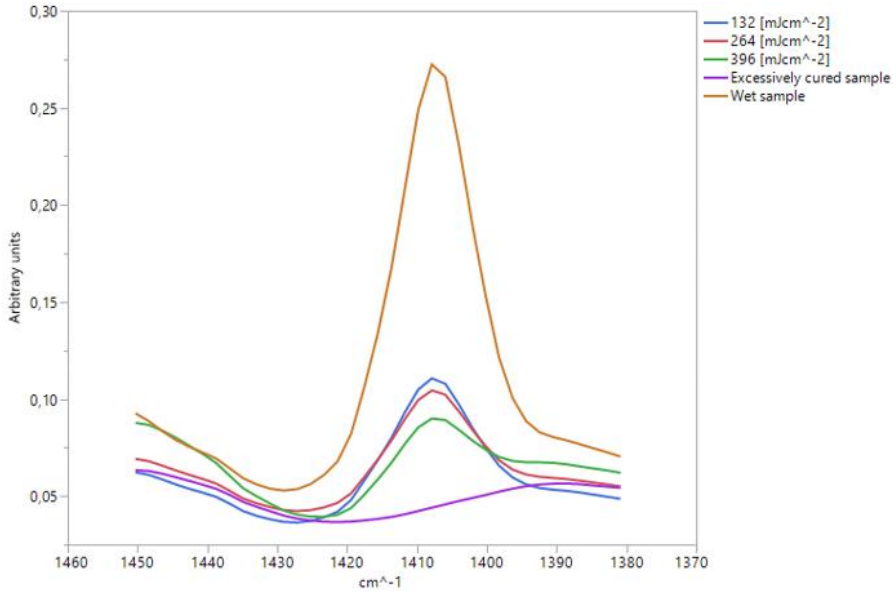

Figure 18. Acrylate absorption band at 1407 cm^{-1} with various grades of curing using 280 nm LED chip.

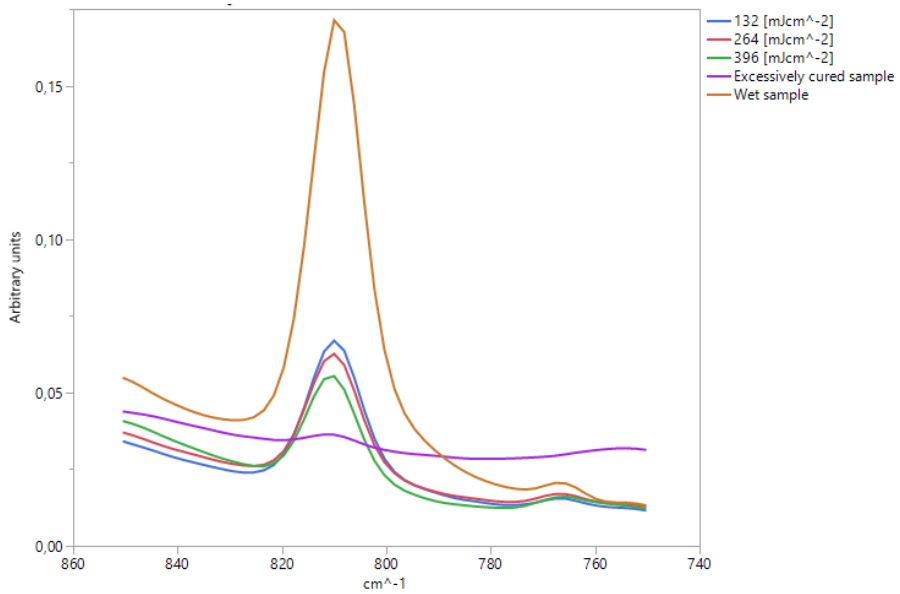

Figure 19. Acrylate absorption band at 810 cm^{-1} with various grades of curing using 280 nm LED chip.

Distinct and high-resolution acrylate reflection peaks are visualized at both wavenumbers with great separation between samples exposed to various doses. The area of each peak systematically decreases with an increase in dose [$mJ \times cm^{-2}$]. These results are encouraging to further apply two-point calibration ATR-FTIR for evaluation of the relative acrylate conversion for cured samples.

Figure 20 shows the relative integrated reflection peak areas, for respective wavenumber, of samples cured by the 280 nm LED at various doses at distances d = 5.3 mm and 15.2 mm. The data contains seven cured LED samples with three repeated measurements at each irradiance and dose level and a reference sample cured with a conventional mercury-doped UV arc lamp.

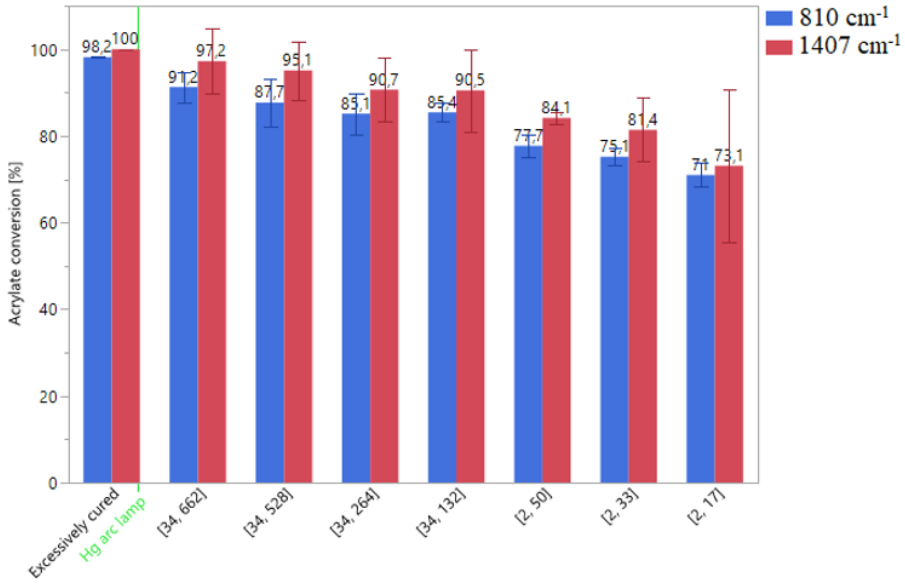

Figure 20. A comparison between calculated acrylate conversion in percentage for wavenumbers 1407 cm^{-1} and 810 cm^{-1}. The reference sample is cured with the mercury arc lamp and the other samples are cured at various irradiance and dose levels ([$mW \times cm^{-2}$, $mJ \times cm^{-2}$]) using a 280 nm LED.

A certain distance between LED chip and applied the film correlates to a certain irradiance which is tabulated in appendix 1. The radiation source on the x-axis is denoted with used irradiance and dose, e.g., [mW×cm^{-2}, mJ×cm^{-2}]. The y-axis denotes the extent of acrylate conversion [%] that highly correlates to the cross-linking density. There is a slight but uniform deviation of the calculated acrylate conversion between the two wavenumbers. However, the 95% confidence interval indicated by the error bars, are clearly wider for data collected at wavenumber 1407 cm^{-1} than 810 cm^{-1}. A F-test could not confirm any significant difference in variance of the measurements done at the respective wavenumber (Appendix 2). However due to the lower standard deviation at wavenumber 810 cm^{-1}, higher precision of the data collected (assumed to be unbiased) is more likely at that wavenumber for iterative measurements, hence the 810 cm^{-1} acrylate absorption peak was decided to be used for all further calculations in this project.

The Martens hardness (HM), and the acrylate conversion dependency by dose are shown in Figure 21 from the same sampling set as described in Figure 20.

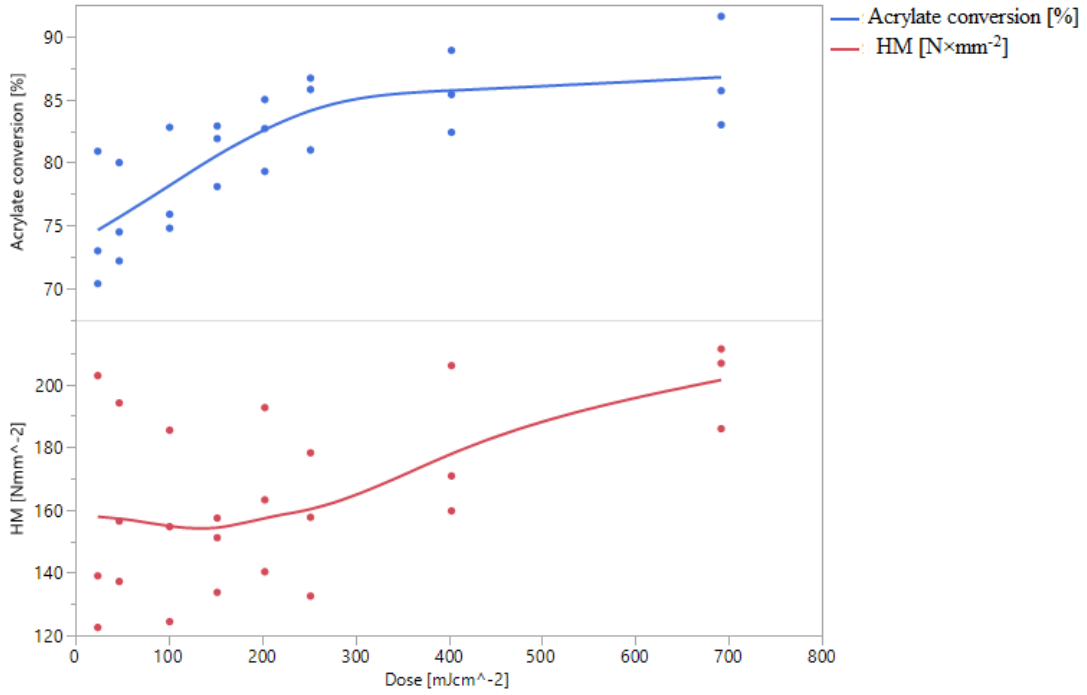

Figure 21. The Martens hardness (HM), and the acrylate conversion dependency on curing dose for sample S1. Smooth spline fit (λ=0.05)

The acrylate conversion follows a clear linear dependence by increased dose until it reaches a plateau around 85%. Increased dose for values over 300 mJ×cm^{-2} increase the acrylate conversion marginally. The HM spread broadly, especially at lower dose levels, but it seems that there is some correlation between hardness and higher dose levels. The widespread data can be explained using a too high indentation load (200 N×mm^{-2}) on to a soft coating since the indentation depth was in the range of 2.5–3.5 µm which exceeds the limits for Bückle's rule. That implies that the glass substrate affects the deformation resistance of the cured film in the measurements performed. Two cycles of micro-hardness measurements are shown in Figure 22. The indentation penetration velocity is clearly not linear which also indicates that the glass substrates is affecting the measurement. Lower indentation load (100 N×mm^{-2}) on the three commercial products which are harder coatings solved the issue.

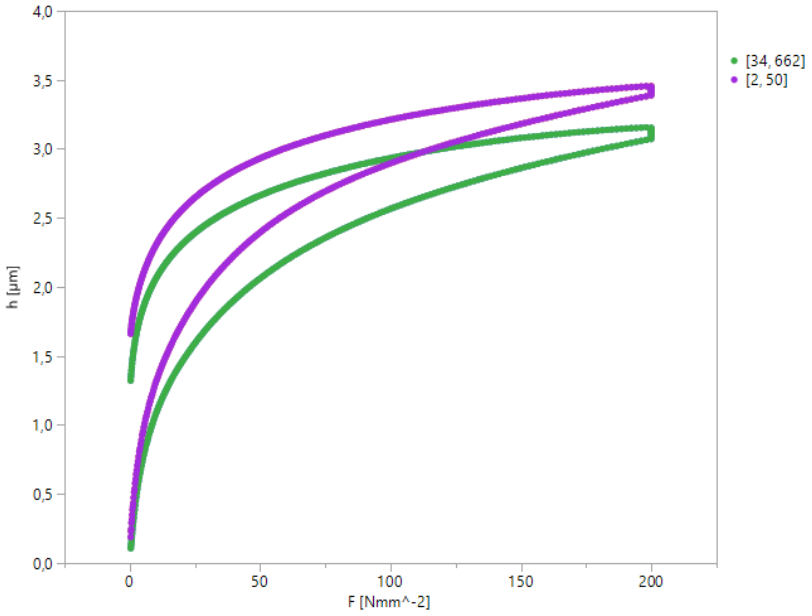

Figure 22. Micro-hardness test on two cured samples [mW×cm^{-2}, mJ×cm^{-2}] from S1. Applied maximum force was 200 N×mm^{-2}/20 s.

The correlation between the two test methods is shown in Figure 23 by a linear fit and summary statistics are presented in Table 5.

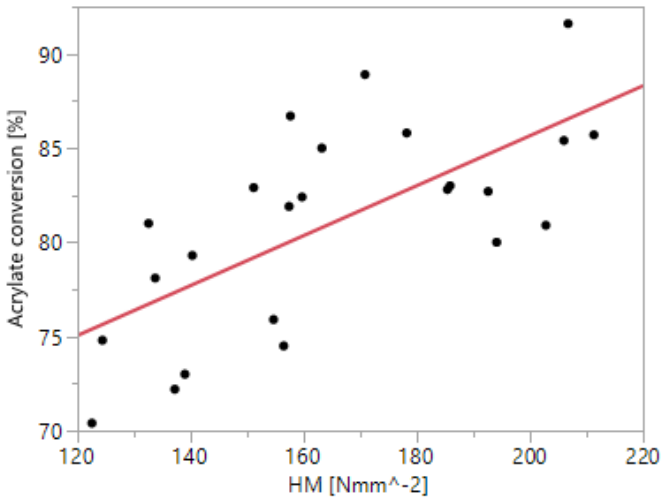

Figure 23. Acrylate conversion [%] vs HM [N×mm^{-2}].

Table 5. Summary statistics.

Summary statistics	Value	Lower 95%	Upper 95%	Significant Probability
Correlation	0.67789	0.377808	0.849094	0.0003
Covariance	102.0816			
Count	24			
R^2	0.459535			

The correlation and covariance show a certain measure of linear dependence and the trend of increasing HM with increasing acrylate conversion is clear.

5.3 Analysis of commercial UV products

Three formulations were chosen as representatives for the commercially relevant and commonly used product types, i.e., pigmented top-coats, pigmented base-coats and clear top-coats.

The results of the three evaluated products are presented individually in this section. The responses that are examined are the extent of conversion of acrylate groups for the top and the bottom of the cured coating film, and the hardness of the same film presented in HM. Model effects are irradiance [$mW \times cm^{-2}$], dose [$mJ \times cm^{-2}$] and type of radiation source (LED/Hg arc lamp). One-way analysis of variance (ANOVA) is used to construct linear models for continuous response data. ANOVA plots with a 95% confidence interval have been constructed. The main goal by this master thesis was to evaluate if curing using short-wavelength UV LED radiation can be compared with the results obtained when curing with a conventional mercury arc lamp. This is highly relevant to understand for the future, when commercially viable short wavelength LED diodes will be available on the market. To further probe this topic, a Dunnett's test has been constructed for each of the three coating types and applied on the results from the curing responses induced by the different LEDs. The curing response at the specified dose according to the quality control (QC) curing test method for the respective product, using a conventional UV mercury arc lamp, was used as the control (α=0.05). Dunnett's test is one type of post hoc test which can be applied after ANOVA. The use of ANOVA in this case would only determine if there were any significant difference between the experimental groups, in this case between the radiation sources at a specific irradiance and dose. That kind of result is of course expected but it would not indicate which group is good enough for a sufficient response by the extent of conversion of acrylate groups at the top/bottom of the film or its hardness. The response that is wanted, is the one measured from samples cured with a mercury arc lamp at a fixed distance with sufficient dose according to the QC control plan. Dunnett's test is restricted to comparing the experimental groups (LEDs) against a single control group (Hg arc lamp) and with 95% confidence, to determine if the curing responses are comparable.

The LEDs of 260 nm and 270 nm did not initiate any notable radical polymerization for any of the three products at the highest possible irradiance and excessive dose, hence not included in any of the presented results. Note that only samples that resulted in surface cure and film formation are presented in the results section, thus only surface cure is not applicable. Measurements that discriminate these limitations due to non-initiating emission wavelengths, or to low irradiance are not included in the report. The x-axis for all the ANOVA and Dunnett's plots in this section, the radiation source is presented with an individual color code and irradiance and dose is given in brackets i.e., [$mW \times cm^{-2}$, $mJ \times cm^{-2}$].

The variation of LED chip, irradiance, and dose (model effects) do not only serve the purpose of finding settings for sufficient cure. It also serves the purpose of constructing linear trends of the responses i.e., for a given LED chip, irradiance, and dose. The constructing profiler in the data analysis software, JMP 14, can visualise which

LED chip(s) that is most effective for each product and what irradiance and dose that is needed to reach the same acrylate conversion and hardness as for curing with the conventional mercury arc lamp according to the products QC control plan.

5.3.1 Pigmented top-coat

The pigmented top-coat only cured using the 290 nm LED chip at the highest registered irradiance (52 mW×cm^{-2}). No initiated curing occurred at 28 mW×cm^{-2} (d=6.9 mm). The curing was performed at doses slightly below

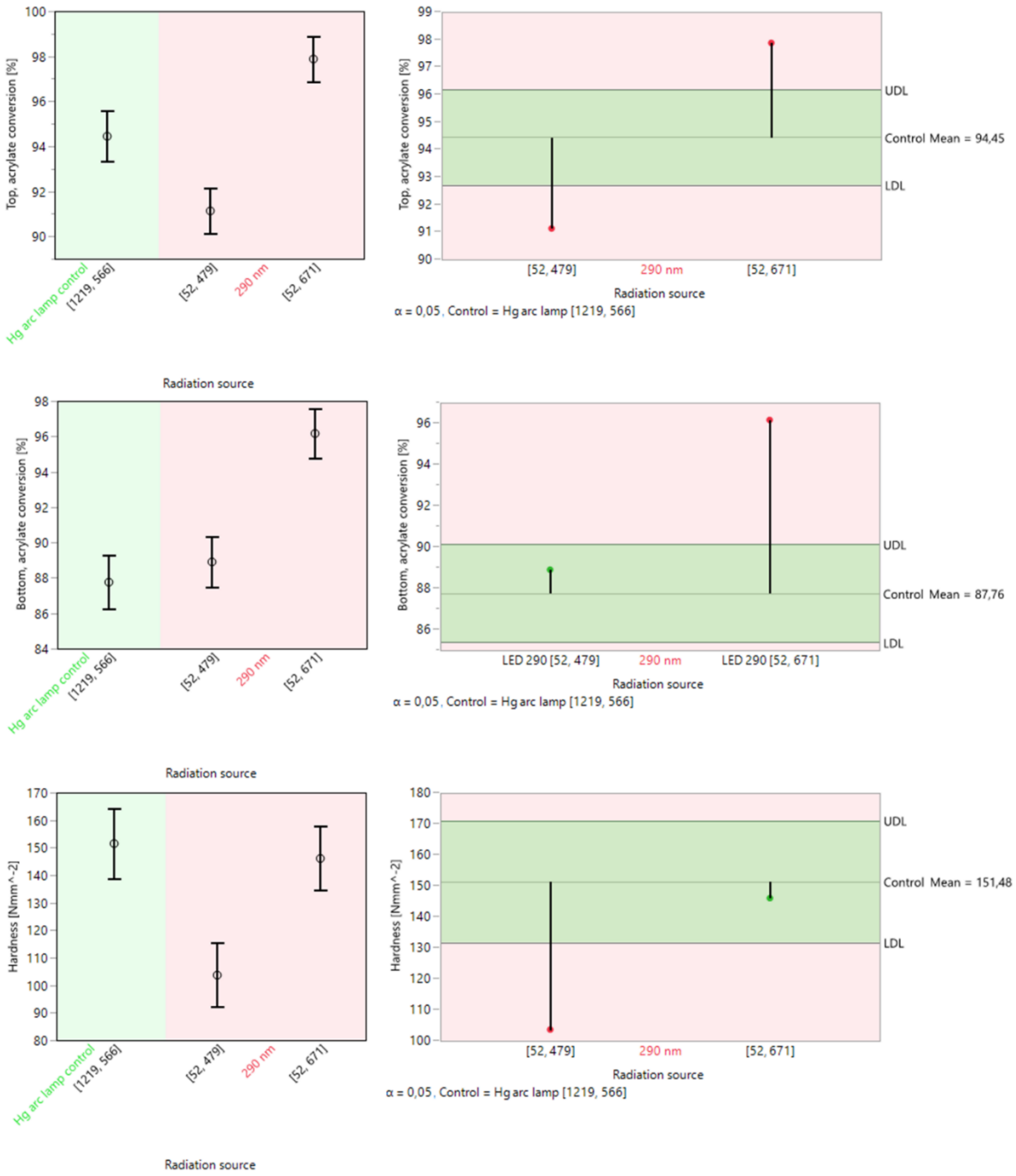

Figure 24. Pigmented top-coat: (Left column) Arithmetic mean plots with 95% confidence interval for the three different responses (y-axis) at various curing (x-axis) denoted on the form: [mW×cm^{-2}, mJ×cm^{-2}]. (Right column) Dunnett's test where the control is a sample cured by the conventional method of mercury arc lamp at dose [566 mJ×cm^{-2}] according to the QC control plan for the product.

(479 mJ×cm^{-2}) and above (671 mJ×cm^{-2}) of the control (two passages; 566 mJ×cm^{-2}) and is presented in Figure 24. The acrylate conversion measured on the top and bottom of the cured films are clearly higher for curing at 671 mJ×cm^{-2} compared to 479 mJ×cm^{-2}, and are also higher than the value of the control measurement on the film cured with the mercury arc lamp. The LED-cured film did also exhibit comparable hardness to the control. The linear model in Figure 25 shows that at the same dose (566 mJ×cm^{-2}) and at irradiance of 52 mW×cm^{-2} for the 290 nm LED chip compared to irradiance of 1219 mW×cm^{-2} for the control, results in acrylate conversions that are at the same level, but the control exhibits a higher hardness. Since curing only occurred at the smallest distance for one LED chip, no irradiance profile for any of the responses can be constructed; however, the hardness deviates significantly at similar extents of acrylate conversion which indicate that the cross-linking process might deviate as well between the mercury arc lamp- and LED curing. This is also a common observation among chemists and technicians working at Sherwin–Williams. Possible explanations could be the low irradiance of the LED chip or/and the low dose by the 395 nm LED unit which is constant (100 mJ×cm^{-2}) for all measurements. Also, due to the fact that the LEDs induce less to no heat, hence reducing the ambient temperature when curing (T_{cure}), which in turn affects the diffusion length of cross-linkers like monomers. Furthermore, the photoactivity of each photoinitiator, induced by a narrow band intensity line from a LED is unknown and assumably could influence the formation of the randomly growing network. The anisotropic curing of the LEDs became visually clear for some samples of both the pigmented coatings (Appendix 4). This could also be a reason for generally lower hardness by LED-cured samples even though the sampling procedure (section 4.3) was thoroughly performed.

However, using slightly higher LED curing energies (52 mW×cm^{-2} and 671 mJ×cm^{-2}) results in even higher acrylate conversion, both on top and bottom of the LED cured film, in combination with equivalent hardness as compared to the reference sample cured with conventional UV arc lamp. This result is encouraging and suggests that conventional curing in this case could be exchanged by LED curing while still maintaining the same properties of the cured film.

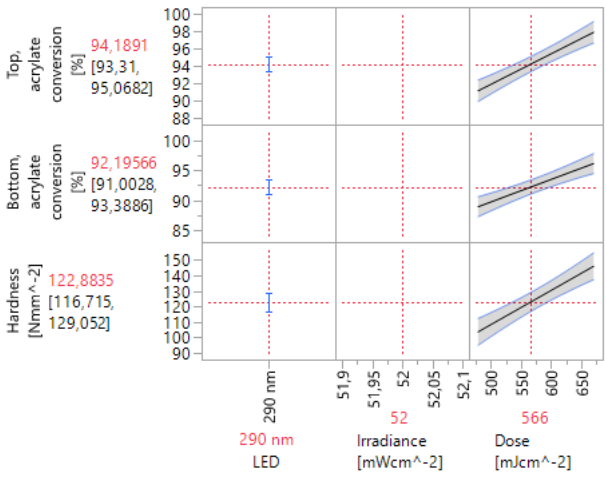

Control response	Reference value
Top, acrylate conversion [%]	94.5
Bottom, acrylate conversion) [%]	87.8
Hardness [N×mm^{-2}]	151.5

Figure 25. Pigmented top-coat: (Left) Profile of the constructed linear trends. Red numbers on the *y*-axis are the expected values of the responses for the fixed settings of irradiance and dose for given LED chip which is shown on the *x*-axis. (Right) Table shows the responses for the film cured by the mercury arc lamp at dose [566 mJ×cm^{-2}] according to the QC control plan for the product.

5.3.2 Pigmented base-coat

The pigmented base-coat was cured by the 280 and 290 nm LEDs at various irradiance and dose settings. It is clear from the LSM and Dunnett's plots that the 280 nm LED is the most effective one. These results are highly expected due to the main absorption peak at 280 nm for the hydroxy acetophenone photoinitiator (type I). That the 290 nm LED chip also induces free-radical polymerisation but exhibits lower response values is in line with the expected partial overlap of the main absorption peak.

Yet again, LED curing results in a high extent of acrylate conversion for both top and bottom of the cured film. At the same dose (283 mJ×cm^{-2}) and a limiting irradiance of 47.8 mW×cm^{-2} LED curing gives equal acrylate conversion but a softer coating than for the control. Same reasoning as for the pigmented top-coat can also be applied here for possible explanations of lower HM values. However, as in the case of the pigmented topcoat, but this time using 280 nm LED encouraging results for LED curing can be seen. Using higher LED curing energies (52 mW×cm^{-2} and 794 mJ×cm^{-2}) results in an equal acrylate conversion, both on top and bottom of the LED cured film, in combination with equivalent hardness as compared to the reference sample cured with conventional UV arc lamp. Again, this result is encouraging and suggests that conventional curing also in this case could be exchanged by LED curing while still maintaining the same properties of the cured film.

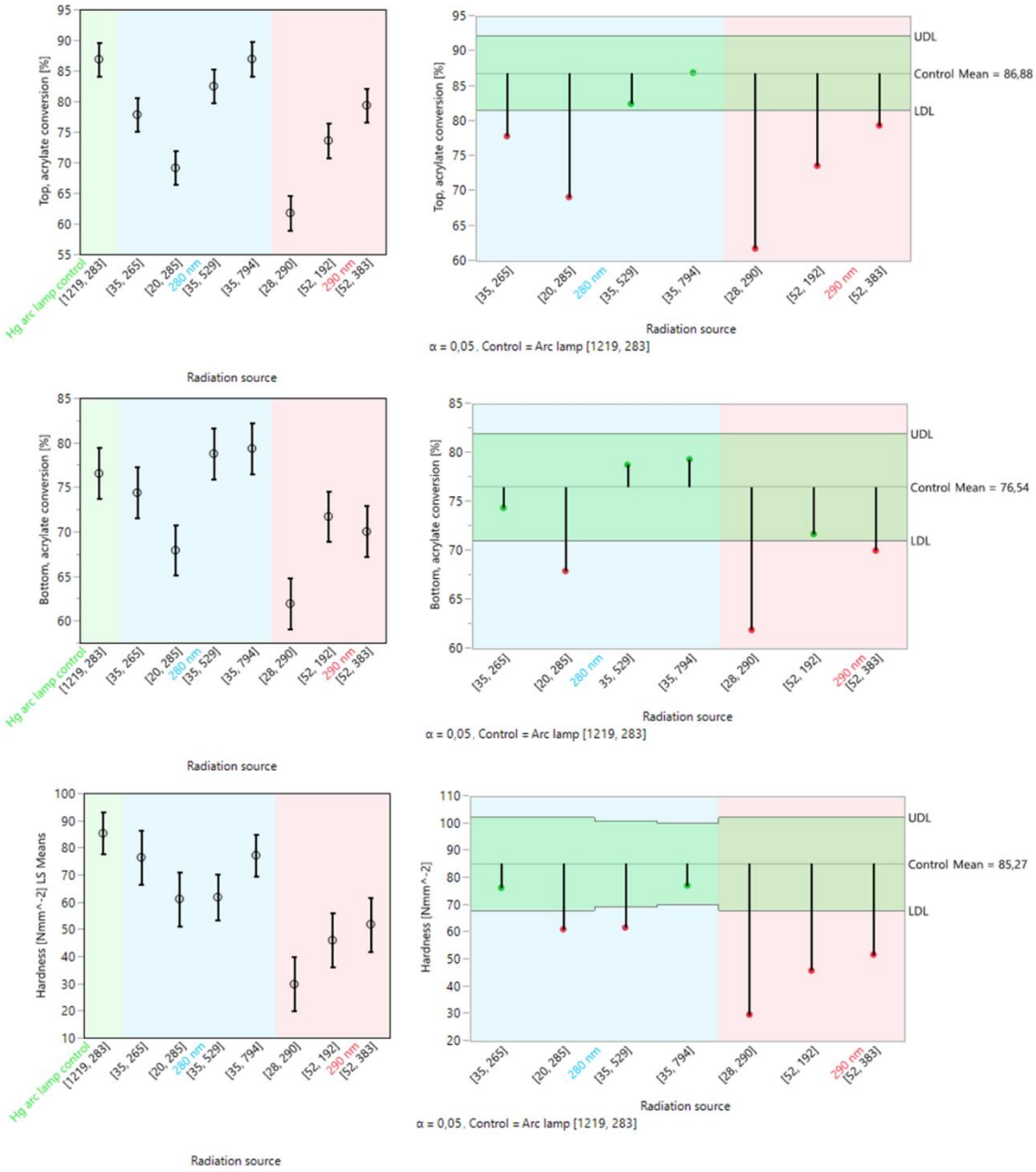

Figure 26. Pigmented base-coat: (Left column) Arithmetic mean plots with 95% confidence interval for the three different responses (y-axis) at various curing (x-axis) denoted on the form: [mW×cm^{-2}, mJ×cm^{-2}]. (Right column) Dunnett's test where the control is a sample cured by the conventional method of mercury arc lamp at dose [283 mJ×cm^{-2}] according to the control plan for the product.

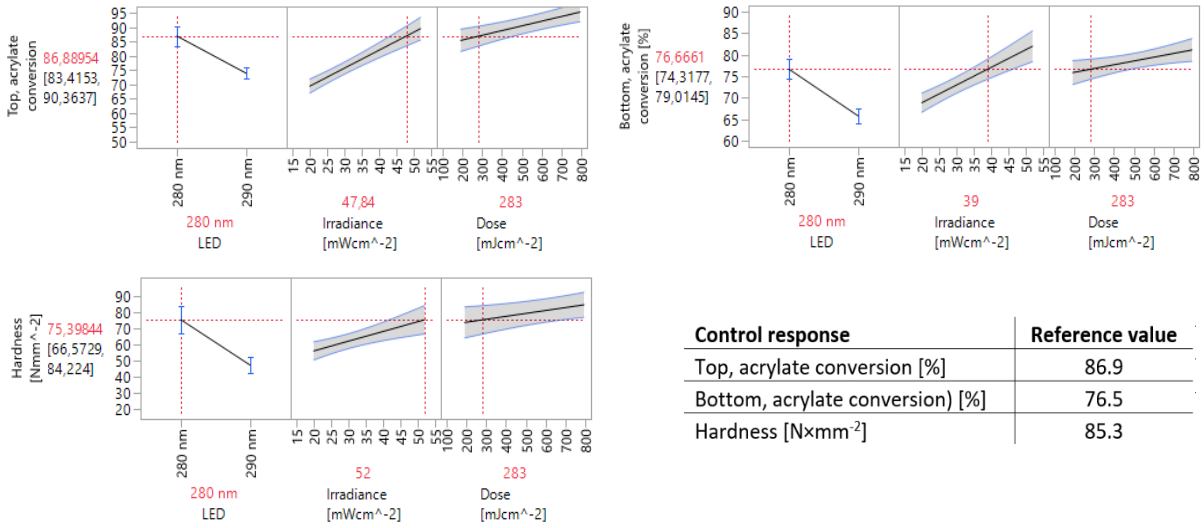

Control response	Reference value
Top, acrylate conversion [%]	86.9
Bottom, acrylate conversion) [%]	76.5
Hardness [N×mm^{-2}]	85.3

Figure 27. Pigmented base-coat: (Left) Profile of the constructed linear trends. Red numbers on the *y*-axis are the expected values of the responses for the fixed settings of irradiance and dose for given LED chip which is shown on the *x*-axis. (Right) Table shows the responses for the film cured by the mercury arc lamp at dose [283 mJ×cm^{-2}] according to the QC control plan for the product.

5.3.3 Clear top-coat

Most of the measurements lie within the confidence interval of the control hence matching the criteria for the control plan of the product. High conversion of acrylate groups using LEDs in the range of 280–320 nm is observed for the surface cure (top) where all curing tests lie well within the control confidence interval and leaning towards the upper limit, indicating a more effective surface cure compared to conventional curing using the mercury arc lamp. The conversion extent at the bottom is leaning towards the lower confidence limit for most measurements, indicating worse penetration depth of LED radiation, and a less effective through cure than for the control. However, most of the curing measurements lie within the control confidence limit and are considered statistically comparable. One should also keep in mind that in these tests, involving the clear topcoat, the 395 nm LED was not used to assist deep cure. The 280 nm LED is deviating from the other LEDs and is probably less effective to excite MBF (type I/type II) since hydroxy acetophenone (type I) should have high photoactivity due to a main absorption peak at 280 nm which also can be related to the high surface cure but lesser bulk cure.

All hardness results are on the same level, or higher, as compared to the conventionally cured sample, except for lowest irradiance and dose setting for the 280 nm LED. The hardness measurements did not show any clear trends on output power of irradiance and dose, but highest values are found for 300- and 310 nm LED while 280 nm is slightly worse. The multi-functionality of binder and monomer explains the high curing rate and degree of acrylate conversion, combined with the absence of any high reflective/absorption pigments like rutile titanium dioxide. Typically, the clear coat is applied at about 5 µm in an industrial line, making it less sensitive to the fact that short-wavelength UV light has less penetration depth than longer-wavelength UV light. On the other hand, the curing process is more sensitive to oxygen inhibition and its low viscosity can lead to higher rates of oxygen diffusion into the coating. The prediction profiler in Figure 29 shows that the LED chip at 300 nm induces the highest response for the product at the same dose (283 mJ×cm^{-2}) as the control combined with an irradiance at 76 mW×cm^{-2} to fulfil the same acrylate conversion for the bottom measurement which is the limiting response factor. The confidence limit for all constructed linear models are wide due to the high level of curing for all measurements that results in very small variations of the response factors which leads to high uncertainties of the linear trends. Again,

as for the pigmented topcoat and basecoat, the results are encouraging for the possibility to completely replace the UV arc lamp with LEDs in the future while maintaining the properties of the cured film.

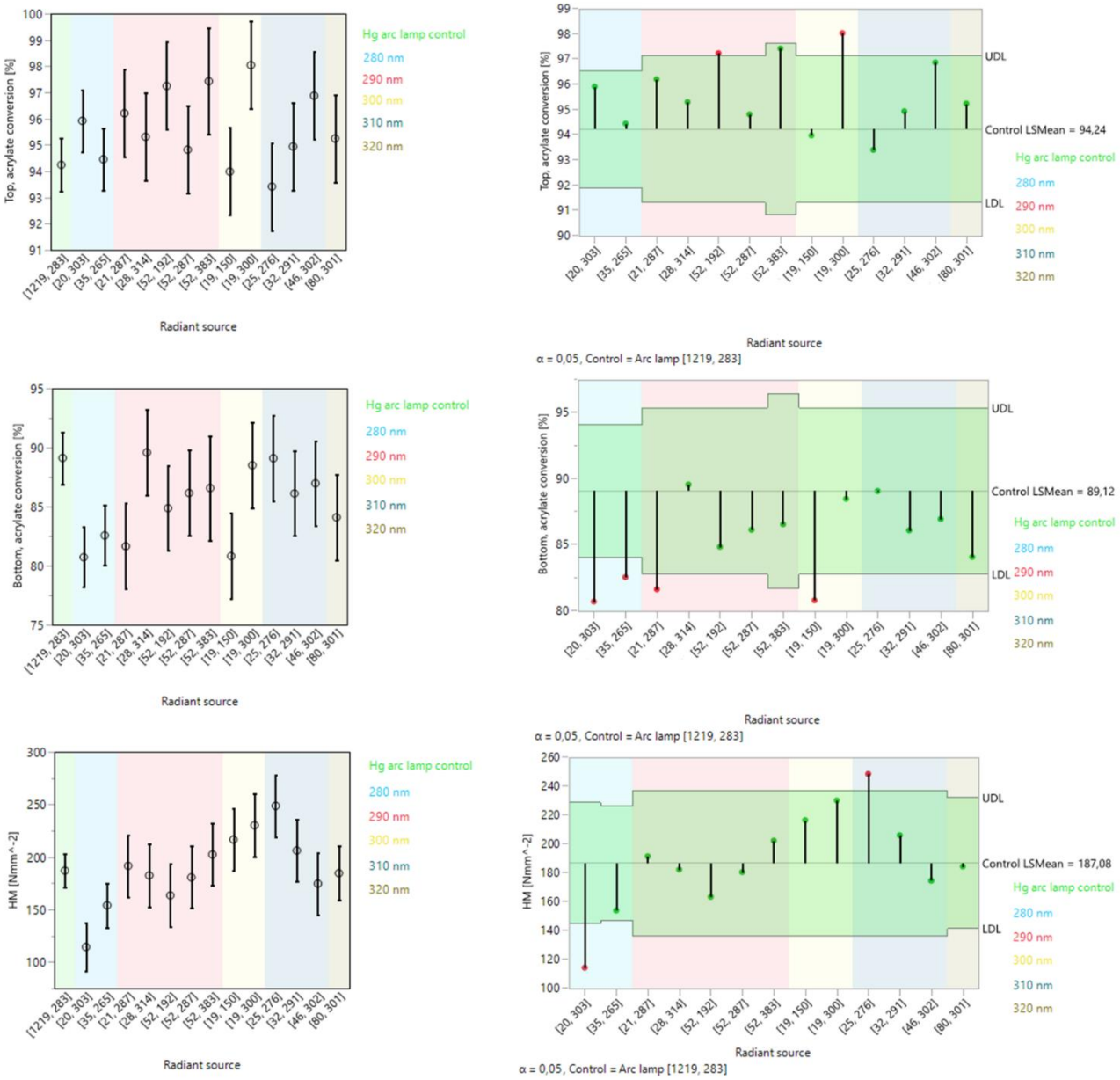

Figure 28. Clear top-coat: (Left column) Arithmetic mean plots with 95% confidence interval for the three different responses (y-axis) at various curing (x-axis) denoted on the form: [mW×cm^{-2}, mJ×cm^{-2}]. (Right column) Dunnett's test where the control is a sample cured by the conventional method of mercury arc lamp at dose [283 mJ×cm^{-2}] according to the control plan for the product.

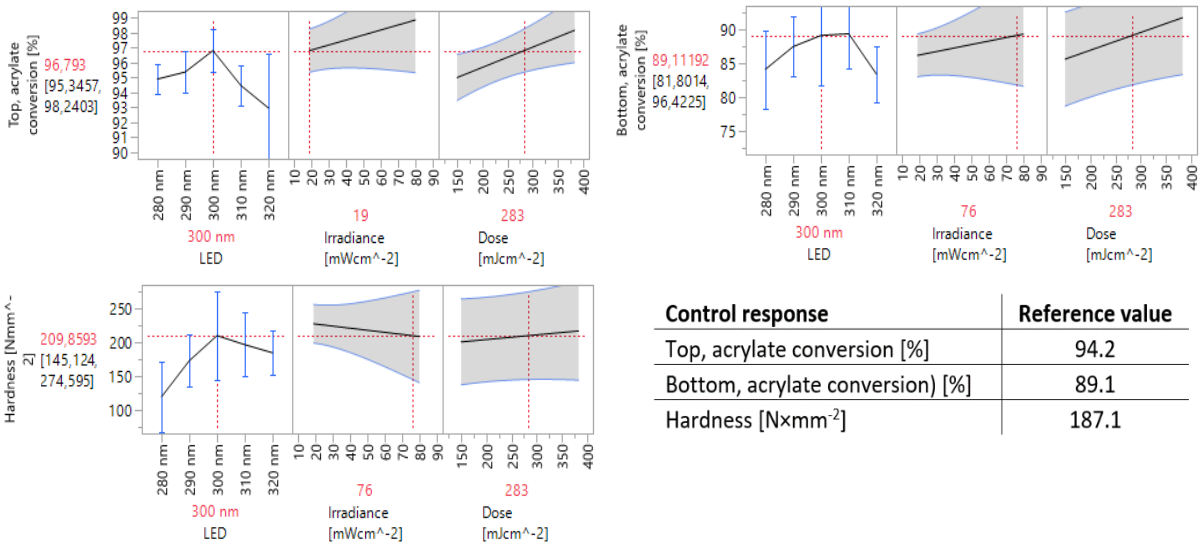

Control response	Reference value
Top, acrylate conversion [%]	94.2
Bottom, acrylate conversion) [%]	89.1
Hardness [N×mm^{-2}]	187.1

Figure 29. Clear top-coat: (Left) Profile of the constructed linear trends. Red numbers on the *y*-axis are the expected values of the responses for the fixed settings of irradiance and dose for given LED chip which is shown on the *x*-axis. (Right) Table shows the responses for the film cured by the mercury arc lamp at dose [283 mJ×cm^{-2}] according to the QC control plan for the product.

5.4. Multivariate analysis

Multivariate data analysis is a powerful tool to detect main trends in large amounts of data that are otherwise hard to overview. Different multivariate methods have been performed in this project, such as principal component analysis and multiple correspondence analysis only to realize that most of the results could be misleading and could in many cases lead to incorrect conclusions. The main reasons are that the three products are very different in their response to curing (as they naturally are due to their different purposes). Same curing settings will give different properties in hardness, acrylate conversion, and many other variables due to their formulation. A multivariate analysis is presented in Table 6 and visualized in a color correspondence plot in Figure 30. According to this analysis, both the irradiance and dose has a negative correlation with hardness and a weak correlation to the extent of acrylate conversion. However, when looking at the responses individually in the profiler plots for each product, there is an overall positive dependence for both irradiance and dose. This can be explained by the highly diverse properties of the products.

Table 6. Multivariate data analysis where $-1 \leq r \geq 1$. No correlation = -1, highest possible correlation = 1.

	Irradiance [mW×cm^{-2}]	Dose [mJ×cm^{-2}]	Top, acrylate conversion [%]	Bottom, acrylate conversion [%]	Hardness [N×mm^{-2}]
Irradiance [mW×cm^{-2}]	1	0.1522	0.2036	0.283	-0.0115
Dose [mJ×cm^{-2}]	0.1522	1	0.1241	0.2862	-0.223
Top, acrylate conversion [%]	0.2036	0.1241	1	0.8629	0.7789
Bottom, acrylate conversion [%]	0.283	0.2862	0.8629	1	0.6854
Hardness [N×mm^{-2}]	-0.0115	-0.223	0.7789	0.6854	1

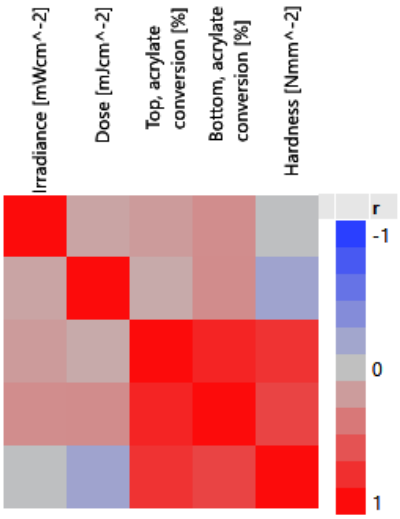

Figure 30. Color correspondence plot. Blue indicates high correlation, red low correlation.

The correlation between hardness, surface acrylate conversion, and bulk acrylate conversion is high and further establishes the correlation shown for the S1 sample in Figure 21 and 23. The whole multivariate analysis is found in Appendix 5, but two of the correlation plots are presented in Figure 31. A smooth spline fit line is drawn through the data and clearly visualizes the hardness dependence of increasing acrylate conversion.

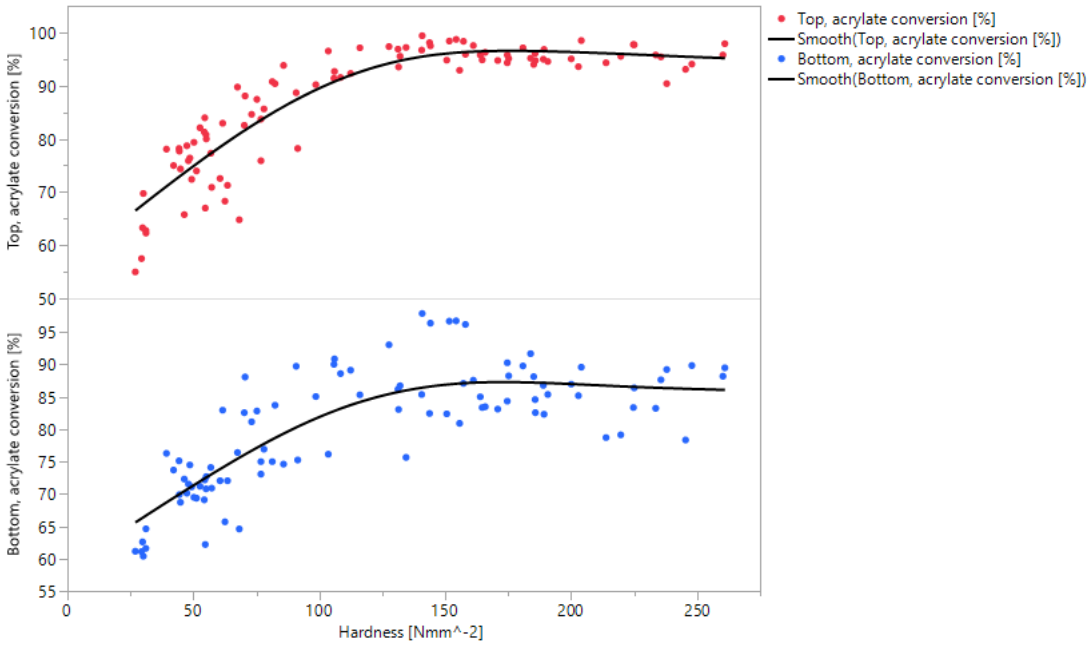

Figure 31. The acrylate conversion [%] vs The Martens hardness (HM) for three commercial products cured at various irradiance [mW×cm^{-2}] and dose [mJ×cm^{-2}].

5.5 Summary

It has been shown that short-wavelength LEDs combined with long-wavelength LEDs can exhibit comparable curing properties to the conventional method of the mercury arc lamp. To understand what peak emission wavelengths that would cover the absorption lines of the broad range of photoinitiators that are in use today, further screening needs to be performed. One must also keep in mind that the short-wavelength LED curing of the coatings has been performed in a stationary manner to enable comparable magnitudes of dose (mJ×cm^{-2}). These experiments have shown, quite unexpectedly, that an irradiance at the order of 20–80 mW×cm^{-2}, depending on product, could be enough for the short-wavelength LEDs to activate proper curing and it is not governed by time-dependency as the dose is. The irradiance is, however, distance-dependent by the inverse-square law (Eq. 3). The distance between the LEDs and the substrate is a key parameter to understand how much higher the radiant flux needs to be for achieving sufficient irradiance. The average radiant intensity, I, i.e., constant K in Figure 14 for the five LEDs constituting the experiment, is approximately ~ 2000 = K_{av}. If K_{av} is solved for an irradiance, E, at 100 mW×cm^{-2} for a given distance, d, at 50 mm and x = 2, the radiant intensity needs to be approximately 125 times larger than the average of the five LEDs. Since the radiant intensity is the radiant flux per solid angle, they have a direct dependency, i.e., the radiant flux needs to be 125 times larger to obtain the right curing properties limited to the irradiance. This estimation is valid if the injection current is the same as in the experiments, i.e., 350 mA, although the radiant flux would increase if the LED structures could be driven at even higher forward-biased currents. If curing occurs at a distance, d at 10 mm, the radiant flux of the LED needs only to be 5 times larger. These estimations give an indication of what order of magnitude the power output must be for a given distance.

The dose is probably the limiting factor for short-wave LEDs due to high belt speeds in industrial lines and the large number of LEDs that is needed. It is not possible to make a fully reasonable calculation of the sufficient radiant flux due to radiant distribution overlap that will be imposed by multiple LEDs and the time dependency. However, an estimate calculation by comparing the dose of the most powerful LED (320 nm) to the curing settings of the mercury arc lamp in Table 3 (belt speed: 27 [m/min], dose: 283 [mJ×cm^{-2}]) results in that a 1.69 m long LED unit is needed that is forward-biased with the same settings as in the experiments by the distance of 5.3 mm between the LED and substrate to achieve the same dose. No radiant distribution overlap is considered in the calculation. Comparing these values, having the same number (216) and configuration of LED chips as of the 395 nm LED unit, a belt speed of 2-3 [m/min] would give the same dose as of the mercury arc lamp for the settings in Table 3. Note that irradiance is not considered here. These estimates are highly simplified and the conclusion about the power output of the LEDs are probably underestimated by these calculations, although they do give some understanding of the current performance of the evaluated LEDs in this project.

6. Conclusions

The aim of this project was to examine if combinations of UVC, UVB and UVA radiation from UV-LEDs could be used as a source for curing acrylate coating systems and be a realistic, mercury-free replacement, of the mercury arc lamp in the future. It has been shown that LEDs are a viable radiation source for UV curing at comparable irradiance and dose to the conventional method of the mercury arc lamp. However, the power output of the LEDs in the range of UVB and UVC are not sufficient to be applied in an industrial line today.

Values of micro-hardness indentation tests and ATR-FTIR measurements have proved to be highly correlated which further establishes that the extent of acrylate conversion is a good estimate of the relative cross-linking density. These results do also prove that both micro-hardness indentation and ATR-FTIR are two robust test methods to be used for cured UV coatings with high reproducibility.

The short-wavelength LEDs have been evaluated on three different commercial products that represent a broad spectrum of features and curing properties of UV paints. The irradiance [$mW \times cm^{-2}$] of the LEDs compared to the conventional mercury arc lamp are relatively low but has proved to be a sufficiently high flux density at examined distances to activate free-radical polymerization for all three formulations at one or several semi-discrete emission wavelengths. Doses [$mJ \times cm^{-2}$] about the same levels used today with the mercury arc lamp, have for some LEDs resulted in even higher acrylate conversion at both the top and the bottom of the cured films for all three products. Both pigmented formulas showed lower values of HM compared to samples cured by the mercury arc lamp at the same level of acrylate conversion. Reasons for this deviation have been discussed extensively. The results that have been obtained in this project are encouraging for the possibility to completely replace the UV mercury arc lamp with LEDs in the future while maintaining the properties of the cured film.

However, the emission of radiant flux (power output) has proved to be insufficient in the sense of practically implementing short-wavelength LEDs today, due to the distance between the radiant source and the substrate where irradiance is limited by the inverse-square law. The dose is consequently insufficient as well and is furthermore influenced by its time-dependency which is relevant in an industrial coating line where high belt speeds are used. Thus, short wavelength LEDs are not a viable radiant source in the UV coating industry today; it could with continued improvements of the LEDs external quantum efficiency and material structures, managing higher current densities, prove to be a highly viable short-wavelength UV radiation source of the future.

7. Future outlooks

If or when short-wave LEDs have improved sufficiently in the UVC/UVB region to be regarded as viable radiation sources, some interesting ways of continuing this research would be:

- Screen viable UVC/UVB LEDs for all commercial photoinitiators currently used at Sherwin–Williams and optimize the number LED peak emission wavelengths matching their main absorption peaks.

- With a fixed number of LED emission wavelengths, they can be examined in similar ways as in this project, by themselves and mixed.

- Cure larger areas of wet paint with several LEDs to achieve isotropic curing.

- Cure larger areas on wood substrate to test crucial properties like adhesion, chemical resistance, wear resistance, gloss, color, abrasion, and scratch resistance.

- Perform UV/VIS spectroscopy on main compounds like binders and calculate absorption for the screened LED semi-discrete emission wavelengths.

Acknowledgements

First, I would like to send my thanks and appreciations to my supervisor Rickard Drougge at Sherwin–Williams for tirelessly correcting the content in this report, the help with experimental execution, and many rewarding discussions. Also, thanks to Jonas Mindemark at Uppsala University for patiently reviewing this report down to every comma and providing valuable input.

Additional thanks to the R&D team at UV-lab for always making me feel at home, hope I will see you all soon. Thanks to Oscar for the practical introduction of ATR-FTIR and microhardness measurements. Thanks to Fredrik for making my life easier with daily obstacles.

REFERENCES

(1) Green, W. A. *Industrial Photoinitiators: A Technical Guide*, Firsr.; Taylor & Francis Group: Boca Raton, US, 2010.

(2) Minamata Convention on Mercury > Home http://www.mercuryconvention.org/Home/tabid/3360/language/en-US/Default.aspx (accessed Nov 28, 2020).

(3) Oppenländer, T. Mercury-Free Sources of VUV/UV Radiation: Application of Modern Excimer Lamps (Excilamps) for Water and Air Treatment. *J. Environ. Eng. Sci.* **2007**, *6* (3), 253–264. https://doi.org/10.1139/S06-059

(4) Auslender, V. L.; Berejka, A. J.; Bol, J. L.; Brinston, R.; Bryazgin, A.; Calvo, W. A. P.; Chmielewski, A.; Cleland, M. R.; Cokragan, A.; Ehlermann, D. A. E.; Fletcher, M.; Guven, O.; Haji-Saeid, M.; Hamm, R. W.; Letournel, E.; Machi, S.; Malcom, F.; Mastro, N. L. de.; Safrany, A.; Sampa, M. H. O.; Tallentire, A.; Testoni, A.; Vroom, D. A.; Whitney, W.; Zimek, Z. Industrial Radiation with Electron Beams and X-Rays. **2011**. 059.

(5) Nobel Foundation. Blue LEDs – Filling the World with New Light [Press Release]. **2014**.

(6) Labsphere. The Radiometry of Light Emitting Diodes https://www.labsphere.com/site/assets/files/2570/the-radiometry-of-light-emitting-diodes-leds.pdf (accessed Mar 5, 2021).

(7) (1) Wicks, Z. W.; Jones, F. N.; Pappas, S. P.; Wicks, D. A. *Organic Coatings: Science and Technology*; John Wiley and Sons, 2006. https://doi.org/10.1002/9780470079072.

(8) Jönsson, S.; Sundell, P. E.; Hultgren, J.; Sheng, D.; Hoyle, C. E. Radiation Chemistry Aspects of Polymerization and Crosslinking. A Review and Future Environmental Trends in "non-Acrylate" Chemistry. *Prog. Org. Coatings* **1996**, *27* (1–4), 107–122. https://doi.org/10.1016/0300-9440(95)00526-9

(9) Hiemenz, P. C.; Lodge, T. *Polymer Chemistry*, second edi.; CRC Press Taylor & Francis Group: Boca Raton, US, **2007**.

(10) Allan, N S, Johnson M S, Oldring P K T, S. S. *Chemistry & Technology of UV & EB Formulation for Coatings, Inks & Paints*, Volume 2.; T, O. P. K., Ed.; SITA Technology: London, UK, **1991**.

(11) Agnarsson. B. *Surface Studies on α – Sapphire for Potential Use in GaN Epitaxial Growth*, KTH: Stockholm, Sweden, **2009**.

(12) Cho, J.; Park, J. H.; Kim, J. K.; Schubert, E. F. White Light-Emitting Diodes: History, Progress, and Future. *Laser Photonics Rev.* **2017**, *11* (2). https://doi.org/10.1002/lpor.201600147.

(13) Are, W. T.; They, H.; Be, C. Peak Irradiance & Energy Density. **2018**. https://discover.phoseon.com/peak-irradiance-energy-density (accessed Mar 5, 2021).

(14) Kim, I.; Kivisaari, P.; Oksanen, J.; Suihkonen, S. Diffusion-Drivens Charge Transport in Light Emitting Devices. *Materials.* **2017**, *10* (12), 1–17. https://doi.org/10.3390/ma10121421.

(15) Zhao, H.; Liu, G.; Tansu, N. Analysis of InGaN-Delta-InN Quantum Wells for Light-Emitting Diodes. *Appl. Phys. Lett.* **2010**, *97* (13), 2010–2013. https://doi.org/10.1063/1.3493188.

(16) Gorai, A.; Panda, S.; Biswas, D. Advantages of InGaN/InGaN Quantum Well Light Emitting Diodes: Better Electron-Hole Overlap and Stable Output. *Optik (Stuttg).* **2017**, *140*, 665–672. https://doi.org/10.1016/j.ijleo.2017.04.086.

(17) Seong, T. Y.; Han, J.; Amano, H.; Morkoç, H. *III-Nitride Based Light Emitting Diodes and Applications*; 2013; Vol. 126. https://doi.org/10.1007/978-94-007-5863-6.

(18) Pieke, S.; Paravia, M. *Measurement of Spectral Radiation in UV Curing Systems*. https://www.mendeley.com/catalogue/3c4839ba-7e67-3cdf-b0f2-451518987214/?utm_source=desktop&utm_medium=1.19.4&utm_campaign=open_catalog&userDocumentId=%7B0c0ee239-8306-4ed7-8244-28b99f799a67%7D (accessed Mar 5, 2021).

(19) Rotem, E. *Measuring LED Power and Irradiance with Calibrated Photodiodes*.Ophir. https://www.electrooptics.com/sites/default/files/content/white-paper/pdfs/PD300RM-3A-IS-LED-accuracy.pdf (accessed Mar 5, 2021).

(20) FT-IR Spectroscopy Attenuated Total Reflectance (ATR) https://cmdis.rpi.edu/sites/default/files/ATR_FTIR.pdf (accessed Feb 11, 2021).

(21) Andrew Chan, K. L.; Kazarian, S. G. Attenuated Total Reflection Fourier-Transform Infrared (ATR-FTIR) Imaging of Tissues and Live Cells. *Chem. Soc. Rev.* **2016**, *45* (7), 1850–1864. https://doi.org/10.1039/c5cs00515a.

(22) Xue, Y.; Patel, A.; Sant, V.; Sant, S. Semiquantitative FTIR Analysis of the Crosslinking Density of Poly(Ester Amide)-Based Thermoset Elastomers. *Macromol. Mater. Eng.* **2016**, *301* (3), 296–305. https://doi.org/10.1002/mame.201500190.

(23) Martinez, L.; Agnely, F.; Leclerc, B.; Siepmann, J.; Cotte, M.; Geiger, S.; Couarraze, G. Cross-Linking of Chitosan and Chitosan/Poly(Ethylene Oxide) Beads: A Theoretical Treatment. *Eur. J. Pharm. Biopharm.* **2007**, *67* (2), 339–348. https://doi.org/10.1016/j.ejpb.2007.02.012.

(24) How Do You Know When Your Varnish or Paint is Cured? https://www.azom.com/article.aspx?ArticleID=6106 (accessed Feb 11, 2021).

(25) Broitman, E. Indentation Hardness Measurements at Macro-, Micro-, and Nanoscale: A Critical Overview. *Tribol. Lett.* **2017**, *65* (1), 1–18. https://doi.org/10.1007/s11249-016-0805-5.

(26) IGM RESINS : Energy curing UV/EB Product finder https://www.igmresins.com/en/products (accessed Feb 11, 2021).

Appendix 1

Dose is measured for 24 seconds at fixed integration time within one distance for reproducible results. Integration time is chosen to maximize saturation at certain distance for a specific LED chip.

LED chip 260 nm

	2	269	5	15	13	236	8	0	0	8
d=5.3 mm	3	234	0	0	5	229	10	0	0	10
	4	233	0	0	5	228	9	0	0	9
	5	206	0	0	4	202	9	0	0	9
		237		**3**	**6**	**227**	**9**	**0**	**0**	**9**
d=6.9 mm	1	126	0	0	2	124	5	0	0	5
	2	123	0	0	2	121	5	0	0	5
	3	124	0	0	2	122	5	0	0	5
		124	**0**	**0**	**2**	**122**	**5**	**0**	**0**	**5**
d=8.3 mm	1	98	0	0	1	97	4	0	0	4
	2	99	0	0	1	98	4	0	0	4
	3	103	0	0	2	101	4	0	0	4
		100	**0**	**0**	**1**	**99**	**4**	**0**	**0**	**4**
d=11.6 mm	1	49	0	0	0	49	2	0	0	2
	2	61	1	2	2	56	2	0	0	2
	3	48	0	0	0	48	2	0	0	2
		53	**0**	**1**	**1**	**51**	**2**	**0**	**0**	**2**
d=15.2 mm	1	51	2	5	3	41	1	0	0	1
	2	28	0	0	0	28	1	0	0	1
	3	75	4	10	6	55	1	0	0	1
		51	**2**	**5**	**3**	**41**	**1**	**0**	**0**	**1**
d=18.5 mm	1	-	-	-	-	-	-	-	-	-
	2	-	-	-	-	-	-	-	-	-
	3	-	-	-	-	-	-	-	-	-
		0	**0**	**0**	**0**	**0**	**0**	**0**	**0**	**0**

LED chip 270 nm

		Dose [mJ×cm^{-2}]	VIS	UVA	UVB	UVC	Irradiance [mW×cm^{-2}]	UVA	UVB	UVC
	1	258	0	0	11	247	10	0	9	10
	2	276	0	0	12	264	11	0	0	11
d=5.3 mm	3	266	0	0	11	255	10	0	0	10
	4	260	0	0	11	249	10	0	0	10
	5	261	0	0	11	250	11	0	0	11
		264		**0**	**11**	**253**	**10**	**0**	**2**	**10**
d=6.9 mm	1	148	0	0	5	143	6	0	0	6
	2	152	0	1	6	145	6	0	0	6
	3	149	0	0	5	144	6	0	0	6
		150	**0**	**0**	**5**	**144**	**6**	**0**	**0**	**6**
d=8.6 mm	1	131	1	3	6	121	5	0	0	5
	2	116	0	0	4	112	4	0	0	4
	3	143	2	6	8	127	5	0	0	5
		130	**1**	**3**	**6**	**120**	**5**	**0**	**0**	**5**
d=11.9 mm	1	56	0	0	1	55	2	0	0	2
	2	58	0	0	1	57	2	0	0	2
	3	56	0	0	1	55	2	0	0	2
		57	**0**	**0**	**1**	**56**	**2**	**0**	**0**	**2**
d=15.2 mm	1	31	0	0	0	31	1	0	0	1
	2	37	0	1	1	35	1	0	0	1
	3	31	0	0	0	31	1	0	0	1
		33	**0**	**0**	**0**	**32**	**1**	**0**	**0**	**1**
d=18.5 mm	1	-	-	-	-	-	-	-	-	-
	2	-	-	-	-	-	-	-	-	-
	3	-	-	-	-	-	-	-	-	-
		0	**0**	**0**	**0**	**0**	**0**	**0**	**0**	**0**

LED chip 280 nm

		Dose [mJ×cm^{-2}]	UVB	UVC	Irradiance [mW×cm^{-2}]	UVB	UVC
	1	773	425	328	34	18	16
	2	831	454	377	37	30	17
***d*=5.3 mm**	3	781	428	353	34	18	16
	4	811	447	364	36	19	17
	5	776	428	348	34	18	16
		794	**436**	**354**	**35**	**21**	**16**
***d*=6.9 mm**	1	451	246	205	20	11	9
	2	432	235	197	19	10	9
	3	481	263	218	21	11	10
		455	**248**	**207**	**20**	**11**	**9**
***d*=8.6 mm**	1	340	185	155	15	8	7
	2	330	180	150	15	8	7
	3	330	181	149	15	8	7
		333	**182**	**151**	**15**	**8**	**7**
***d*=11.9 mm**	1	175	95	80	7	4	3
	2	174	95	79	7	4	3
	3	175	95	80	7	4	3
		175	**95**	**80**	**7**	**4**	**3**
***d*=15.2 mm**	1	99	54	45	4	2	2
	2	100	54	46	4	2	2
	3	101	55	46	4	2	2
		100	**54**	**46**	**4**	**2**	**2**
***d*=18.5 mm**	1	63	34	29	2	1	1
	2	64	34	30	2	1	1
	3	61	33	28	2	1	1
		63	**34**	**29**	**2**	**1**	**1**

LED chip 290 nm

		Dose [mJ×cm^{-2}]	UVA	UVB	UVC	Irradiance [mW×cm^{-2}]	UVA	UVB	UVC
	1	1212	2	1094	116	54	0	49	5
	2	1073	2	968	103	50	0	45	5
***d*=5.3 mm**	3	1165	2	1053	110	52	0	47	5
	4	1152	2	1041	109	52	0	47	5
	5	1142	2	1032	108	52	0	47	5
		1149	**2**	**1038**	**109**	**52**	**0**	**47**	**5**
***d*=6.9 mm**	1	614	0	557	57	27	0	25	2
	2	639	0	580	59	29	0	26	3
	3	631	0	572	59	27	0	25	2
		628	**0**	**570**	**58**	**28**	**0**	**25**	**2**
***d*=8.6 mm**	1	481	1	436	44	20	0	18	2
	2	496	1	448	47	21	0	19	2
	3	499	2	448	49	21	0	19	2
		492	**1**	**444**	**47**	**21**	**0**	**19**	**2**
***d*=11.9 mm**	1	234	0	213	21	10	0	9	1
	2	242	0	220	22	10	0	9	1
	3	248	0	225	23	10	0	9	1
		241	**0**	**219**	**22**	**10**	**0**	**9**	**1**
***d*=15.2 mm**	1	146	0	132	14	5	0	5	0
	2	137	0	125	12	5	0	5	0
	3	154	0	137	16	5	0	5	0
		146	**0**	**131**	**14**	**5**	**0**	**5**	**0**
***d*=18.5 mm**	1	88	0	81	7	3	0	3	0
	2	90		82	0	3	0	3	0
	3	83	0	76	7	3	0	3	0
		87	**0**	**80**	**5**	**3**	**0**	**3**	**0**

LED chip 300 nm

		Dose [mJ×cm^{-2}]	UVA	UVB	UVC	Irradiance [mW×cm^{-2}]	UVA	UVB	UVC	UVC
	1	471	0	26	444	1	20	1	19	0
	2	418	0	23	395	0	18	1	18	0
***d*=5.3 mm**	3	460	0	26	433	1	20	1	19	0
	4	441	0	25	415	1	19	1	18	0
	5	466	0	26	440	0	20	1	19	0
		451		**25**	**425**	**1**	**19**	**1**	**19**	**0**
***d*=6.9 mm**	1	293	1	19	264	9	11	0	11	0
	2	286	2	21	246	17	10	0	10	0
	3	275	0	15	260	0	11	0	11	0
		285	**1**	**18**	**257**	**9**	**11**	**0**	**11**	**0**
***d*=8.6 mm**	1	198	0	10	188	0	8	0	8	0
	2	202	0	11	191	0	8	0	8	0
	3	200	0	11	189	0	8	0	8	0
		200	**0**	**11**	**189**	**0**	**8**	**0**	**8**	**0**
***d*=11.9 mm**	1	112	0	5	107	0	4	0	4	0
	2	106	0	5	101	0	4	0	4	0
	3	109	0	5	104	0	4	0	4	0
		109	**0**	**5**	**104**	**0**	**4**	**0**	**4**	**0**
***d*=15.2 mm**	1	65	0	3	62	0	2	0	2	0
	2	66	0	3	62	1	2	0	2	0
	3	65	0	2	63	0	2	0	2	0
		65	**0**	**3**	**62**	**0**	**2**	**0**	**2**	**0**

***d*=18.5 mm**	1	49	0	3	42	4	1	0	1	0
	2	42	0	1	41	0	1	0	1	0
	3	55	1	5	41	8	1	0	1	0
		49	**0**	**3**	**41**	**4**	**1**	**0**	**1**	**0**

LED chip 310 nm

		Dose [mJ×cm^{-2}]	UVA	UVB	UVC	Irradiance [mW×cm^{-2}]	UVA	UVB	UVC	UVC
	1	1058	0	224	834	0	48	10	38	0
	2	1102	0	233	869	0	49	10	39	0
***d*=5.3 mm**	3	959	0	205	754	0	44	9	35	0
	4	1015	0	217	798	0	45	9	36	0
	5	1047	0	224	823	0	46	9	37	0
		1036		**221**	**816**	**0**	**46**	**9**	**37**	**0**
***d*=6.9 mm**	1	745	0	161	584	0	33	7	26	0
	2	625	0	134	491	0	31	7	24	0
	3	728	0	157	571	0	32	7	25	0
		699	**0**	**151**	**549**	**0**	**32**	**7**	**25**	**0**
***d*=8.6 mm**	1	552	0	118	434	0	25	5	20	0
	2	545	0	118	427	0	24	5	19	0
	3	556	0	119	437	0	25	5	20	0
		551	**0**	**118**	**433**	**0**	**25**	**5**	**20**	**0**
***d*=11.9 mm**	1	304	0	66	238	0	12	2	10	0
	2	305	0	66	239	0	12	2	10	0
	3	279	0	60	219	0	11	2	9	0
		296	**0**	**64**	**232**	**0**	**12**	**2**	**10**	**0**

***d*=15.2 mm**	1	178	0	38	140	0	7	1	6	0
	2	174	0	37	137	0	7	1	6	0
	3	175	0	38	137	0	6	1	5	0
		176	**0**	**38**	**138**	**0**	**7**	**1**	**6**	**0**
***d*=18.5 mm**	1	122	0	26	93	3	5	1	4	0
	2	115	0	24	91	0	5	1	4	0
	3	127	1	27	92	7	5	1	3	0
		121	**0**	**26**	**92**	**3**	**5**	**1**	**4**	**0**

LED chip 320 nm

		Dose [mJ×cm^{-2}]	UVA	UVB	UVC	Irradiance [mW×cm^{-2}]	UVA	UVB	UVC	UVC
	1	1882	0	782	1100	0	83	34	49	0
	2	1786	0	749	1037	0	77	32	45	0
***d*=5.3 mm**	3	1827	0	764	1063	0	80	33	47	0
	4	1890	0	791	1099	0	83	34	49	0
	5	1656	0	687	969	0	79	32	47	0
		1808		**755**	**1054**	**0**	**80**	**33**	**47**	**0**
***d*=6.9 mm**	1	1112	0	467	645	0	49	20	29	0
	2	1058	0	445	613	0	47	20	27	0
	3	1105	0	466	639	0	50	21	29	0
		1092	**0**	**459**	**632**	**0**	**49**	**20**	**28**	**0**
***d*=8.6 mm**	1	765	0	323	442	0	34	14	20	0
	2	735	0	310	425	0	33	14	19	0
	3	752	0	317	435	0	33	14	19	0
		751	**0**	**317**	**434**	**0**	**33**	**14**	**19**	**0**

***d*=11.9 mm**	1	368	0	156	212	0	15	6	9	0
	2	362	0	153	209	0	15	6	9	0
	3	368	0	155	213	0	15	6	9	0
		366	**0**	**155**	**211**	**0**	**15**	**6**	**9**	**0**
***d*=15.2 mm**	1	237	3	92	119	23	8	3	5	0
	2	197	0	83	114	0	8	3	5	0
	3	261	5	98	122	36	8	3	5	0
		232	**3**	**91**	**118**	**20**	**8**	**3**	**5**	**0**
***d*=18,2 mm**	1	124	0	52	72	0	5	2	3	0
	2	127	0	53	74	0	5	2	3	0
	3	123	0	52	71	0	5	2	3	0
		125	**0**	**52**	**72**	**0**	**5**	**2**	**3**	**0**

Appendix 2

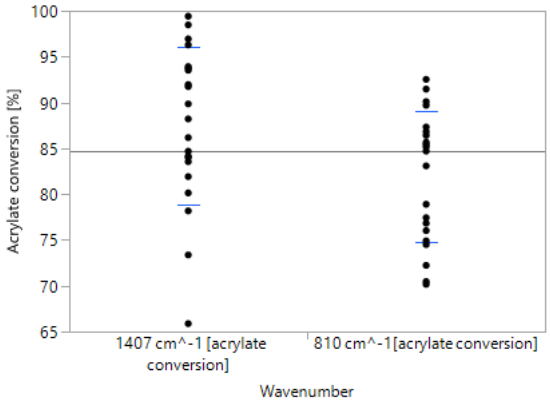

F-test

Test that Variance are equal (α=0.05)

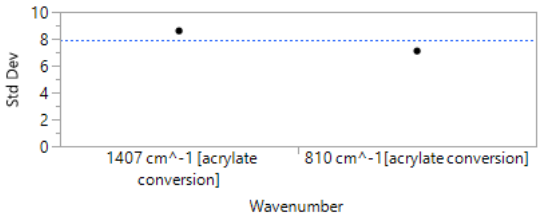

Level	Count	Std Dev	MeanAbsDif to Mean	MeanAbsDif to Median
1407 cm^-1 [acrylate conversion]	21	8,594226	6,884548	6,847512
810 cm^-1[acrylate conversion]	21	7,098287	6,249163	6,002260

Test	F Ratio	DFNum	DFDen	p-Value
O'Brien[.5]	0,7846	1	40	0,3810
Brown-Forsythe	0,3256	1	40	0,5715
Levene	0,2533	1	40	0,6175
Bartlett	0,7093	1	.	0,3997
F Test 2-sided	1,4659	20	20	0,3997

Welch's test

F Ratio	DFNum	DFDen	Prob > F
5,1812	1	38,621	0,0285*

Appendix 3

Paired t-test between two different applications of the same product (clear topcoat & pigmented basecoat) which are applied and cured equally. Normal distribution is assumed by QQ-plot for the whole range of data (acrylate conversion and hardness) for that product where cross-linking density and hardness are centred by curing properties i.e., dose and irradiance.

Clear top-coat

Top

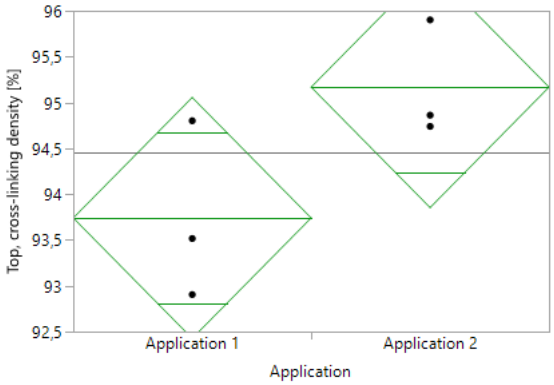

ONEWAY ANALYSIS OF CROSS-LINKING DENSITY (TOP)

Summary of Fit

Rsquare	0,531915
Adj Rsquare	0,414894
Root Mean Square Error	0,819815
Mean of Response	94,45464
Observations (or Sum Wgts)	6

Pooled t-test

Difference	1,4271	t Ratio	2,132007
Std Err Dif	0,6694	DF	4
Upper CL Dif	3,2856	Prob > |t|	0,1
Lower CL Dif	-0,4314	Prob > t	0,05
Confidence	0,95	Prob < t	0,95

Analysis of Variance

Source	DF	Sum of Squares	Mean Square	F Ratio	Prob > F
Application	1	3,054987	3,05499	4,5455	0,1
Error	4	2,688388	0,6721		
C. Total	5	5,743375			

Means for Oneway ANOVA

Level	Number	Mean	Std Error	Lower 95%	Upper 95%
Application 1	3	93,7411	0,47332	92,427	95,055
Application 2	3	95,1682	0,47332	93,854	96,482

Bottom

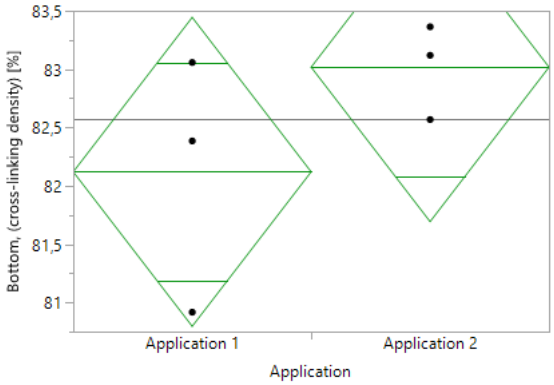

ONEWAY ANALYSIS OF CROSSLINKING-DENSITY (BOTTOM)

Summary of Fit

Rsquare	0,306717
Adj Rsquare	0,133397
Root Mean Square Error	0,825877
Mean of Response	82,56881
Observations (or Sum Wgts)	6

Pooled t-test

Difference	0,897	t Ratio	1,330283
Std Err Dif	0,6743	DF	4
Upper CL Dif	2,7693	Prob > |t|	0,2542
Lower CL Dif	-0,9752	Prob > t	0,1271
Confidence	0,95	Prob < t	0,8729

Analysis of Variance

Source	DF	Sum of Squares	Mean Square	F Ratio	Prob > F
Application	1	1,207032	1,20703	1,7697	0,2542
Error	4	2,72829	0,68207		
C. Total	5	3,935322			

Means for Oneway ANOVA

Level	Number	Mean	Std Error	Lower 95%	Upper 95%
Application 1	3	82,1203	0,47682	80,796	83,444
Application 2	3	83,0173	0,47682	81,693	84,341

Hardness

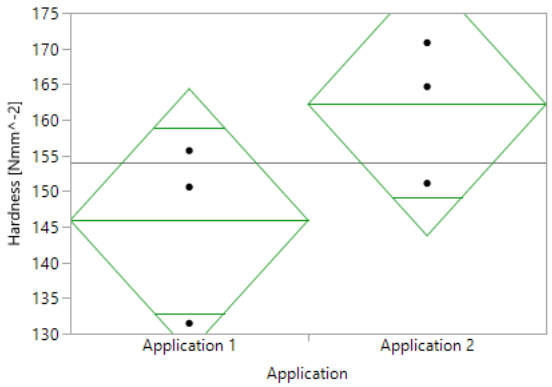

HARDNESS

Summary of Fit

Rsquare	0,428955
Adj Rsquare	0,286194
Root Mean Square Error	11,50692
Mean of Response	154,048
Observations (or Sum Wgts)	6

Pooled t-test

Difference	16,286	t Ratio	1,733409
Std Err Dif	9,395	DF	4
Upper CL Dif	42,372	Prob > |t|	0,1581

Lower CL Dif	-9,8	Prob > t	0,079
Confidence	0,95	Prob < t	0,921

Analysis of Variance

Source	DF	Sum of Squares	Mean Square	F Ratio	Prob > F
Application	1	397,8507	397,851	3,0047	0,1581
Error	4	529,6369	132,409		
C. Total	5	927,4875			

Means for Oneway ANOVA

Level	Number	Mean	Std Error	Lower 95%	Upper 95%
Application 1	3	145,905	6,6435	127,46	164,35
Application 2	3	162,191	6,6435	143,75	180,64

Pigmented base-coat

Top

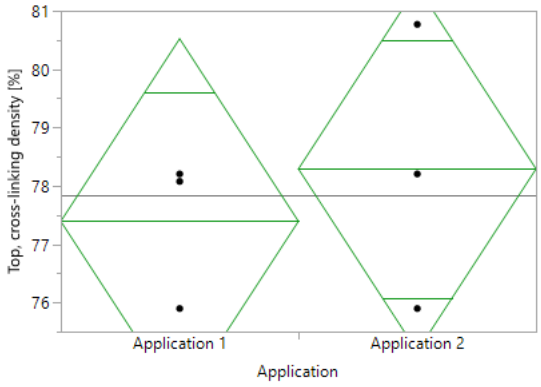

26 ONEWAY ANALYSIS OF CROSSLINKING-DENSITY (TOP)

Summary of Fit

Rsquare	0,073439
Adj Rsquare	-0,1582
Root Mean Square Error	1,952061
Mean of Response	77,84188
Observations (or Sum Wgts)	6

Pooled t-test

Difference	0,8974	t Ratio	0,563061
Std Err Dif	1,5939	DF	4
Upper CL Dif	5,3227	Prob > |t|	0,6035
Lower CL Dif	-3,5278	Prob > t	0,3017
Confidence	0,95	Prob < t	0,6983

Analysis of Variance

Source	DF	Sum of Squares	Mean Square	F Ratio	Prob > F
Application	1	1,208087	1,20809	0,317	0,6035
Error	4	15,24217	3,81054		
C. Total	5	16,45025			

Means for Oneway ANOVA

Level	Number	Mean	Std Error	Lower 95%	Upper 95%
Application 1	3	77,3932	1,127	74,264	80,522
Application 2	3	78,2906	1,127	75,161	81,42

Bottom

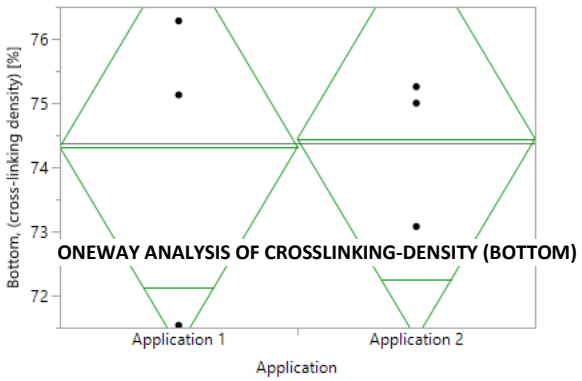

Summary of Fit

Rsquare	0,001633
Adj Rsquare	-0,24796
Root Mean Square Error	1,941507
Mean of Response	74,38034
Observations (or Sum Wgts)	6

Pooled t-test

Difference	0,1282	t Ratio	0,080875
Std Err Dif	1,5852	DF	4
Upper CL Dif	4,5295	Prob > |t|	0,9394
Lower CL Dif	-4,2731	Prob > t	0,4697
Confidence	0,95	Prob < t	0,5303

Analysis of Variance

Source	DF	Sum of Squares	Mean Square	F Ratio	Prob > F
Application	1	0,024655	0,02465	0,0065	0,9394
Error	4	15,0778	3,76945		
C. Total	5	15,10246			

Means for Oneway ANOVA

Level	Number	Mean	Std Error	Lower 95%	Upper 95%
Application 1	3	74,3162	1,1209	71,204	77,428
Application 2	3	74,4444	1,1209	71,332	77,557

Hardness

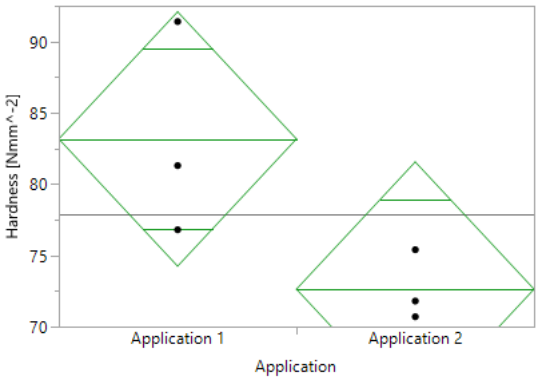

HARDNESS

Summary of Fit

Rsquare	0,573253
Adj Rsquare	0,466566
Root Mean Square Error	5,565369

Mean of Response	77,9
Observations (or Sum Wgts)	6

Pooled t-test

Difference	-10,533	t Ratio	-2,31802
Std Err Dif	4,544	DF	4
Upper CL Dif	2,083	Prob > |t|	0,0813
Lower CL Dif	-23,15	Prob > t	0,9593
Confidence	0,95	Prob < t	0,0407

Analysis of Variance

Source	DF	Sum of Squares	Mean Square	F Ratio	Prob > F
Application	1	166,4267	166,427	5,3732	0,0813
Error	4	123,8933	30,973		
C. Total	5	290,32			

Means for Oneway ANOVA

Level	Number	Mean	Std Error	Lower 95%	Upper 95%
Application 1	3	83,1667	3,2132	74,245	92,088
Application 2	3	72,6333	3,2132	63,712	81,555

Appendix 3.1

Normal Quantile plots for cross-linking density and hardness centred by curing properties.

Clear top-coat

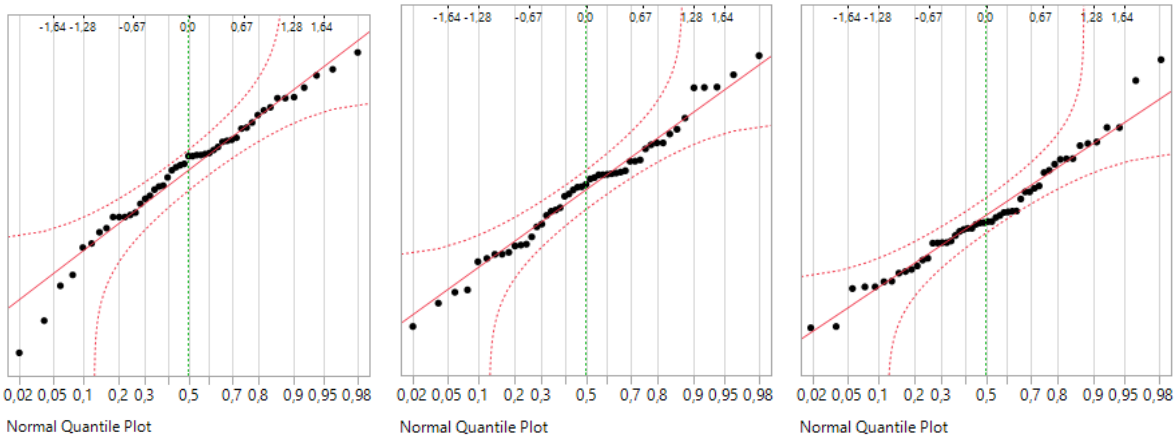

NQP CROSS-LINKING DENSITY (TOP) **NQP CROSS-LINKING DENSITY (BOTTOM)** **NQP HARDNESS**

Pigmented base-coat

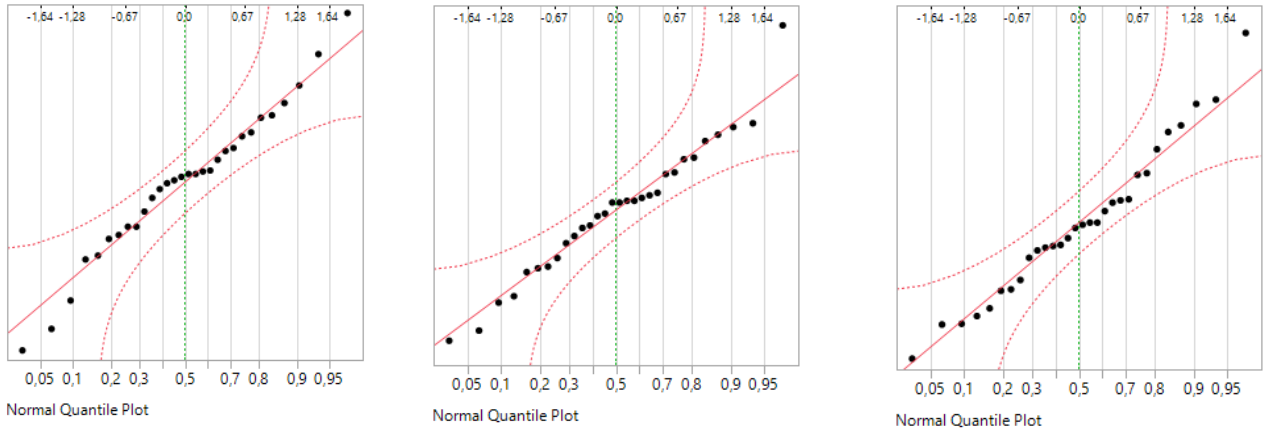

NQP CROSS-LINKING DENSITY (TOP) **NQP CROSS-LINKING DENSITY (BOTTOM)** **27 NQP MICRO-HARDNESS**

Appendix 4

Examples on the anisotropic cured areas of pigmented base- and topcoat.

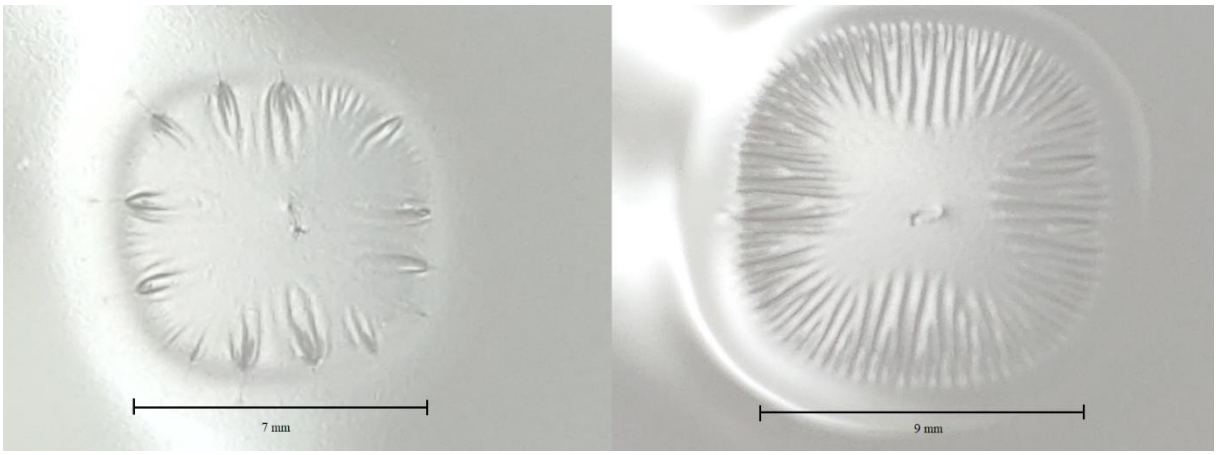
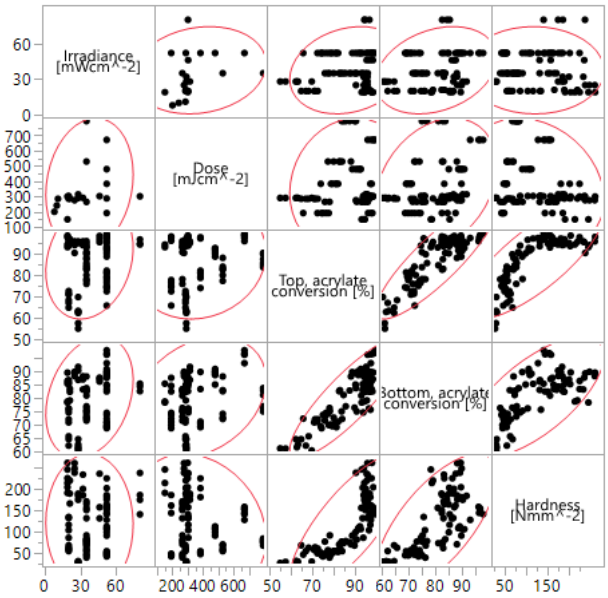
Appendix 5